Paleoceanography and Paleoclimatology

RESEARCH ARTICLE
10.1029/2023PA004690

A Systematic Role for Extreme Ocean-Atmosphere Oscillations in the Development of Glacial Conditions Since the Mid Pleistocene Transition

Stephen Barker[1] **and Gregor Knorr**[2]

[1]School of Earth and Environmental Sciences, Cardiff University, Cardiff, UK, [2]Alfred Wegener Institute (AWI) Helmholtz Center for Polar and Marine Research, Bremerhaven, Germany

Key Points:

- Extreme interstadial-like millennial-scale Antarctic cooling systematically preceded transitions to a glacial state throughout the past 800 kyr
- Such cooling could promote glacial ocean stratification by volume expansion and or salinification of southern-sourced deep waters
- These dynamics can explain the abrupt nature of interglacial-glacial changes in for example, CO_2 since the Mid Pleistocene Transition but apparently not before

Supporting Information:

Supporting Information may be found in the online version of this article.

Correspondence to:

S. Barker and G. Knorr,
barkers3@cf.ac.uk;
Gregor.Knorr@awi.de

Citation:

Barker, S., & Knorr, G. (2023). A systematic role for extreme ocean-atmosphere oscillations in the development of glacial conditions since the Mid Pleistocene Transition. *Paleoceanography and Paleoclimatology*, *38*, e2023PA004690. https://doi.org/10.1029/2023PA004690

Received 25 MAY 2023
Accepted 5 DEC 2023

Author Contributions:

Conceptualization: Stephen Barker, Gregor Knorr
Formal analysis: Stephen Barker
Methodology: Stephen Barker
Validation: Stephen Barker, Gregor Knorr
Writing – original draft: Stephen Barker, Gregor Knorr
Writing – review & editing: Stephen Barker, Gregor Knorr

Abstract We introduce a new hypothesis concerning the role of internal climate dynamics in the non-linear transitions from interglacial to glacial (IG-G) state since the Mid Pleistocene Transition (MPT). These transitions encompass large and abrupt changes in atmospheric CO_2, ice volume, and temperature that we suggest involve critical interactions between insolation and high amplitude oscillations in ocean/atmosphere circulation patterns. Specifically, we highlight the large amplitude of millennial-scale climate oscillations across the transition from Marine Isotope Stage (MIS) 5 to 4, which we argue led to amplified cooling of the deep ocean and we demonstrate that analogous episodes of extreme cooling systematically preceded glacial periods of the last 800 kyr. We suggest that such cooling necessitates a reconfiguration of the deep ocean to avoid a density paradox between northern and southern-sourced deep waters (SSW), which could be accomplished by increasing the relative volume and or salinity of SSW, thus providing the necessary storage capacity for the subsequent (delayed) and relatively abrupt drawdown of CO_2. We therefore explain the transient decoupling of Antarctic temperature from CO_2 across MIS 5/4 as a direct consequence of millennial activity at that time. We further show that similar climatic decoupling typically occurred during times of low obliquity and was a ubiquitous feature of IG-G transitions over the past 800 kyr, producing the appearance of bimodality in records of CO_2, benthic $\delta^{18}O$ and others. Finally we argue that the apparent lack of bimodality in the pre-MPT record of benthic $\delta^{18}O$ implies that the dynamics associated with IG-G transitions changed across the MPT.

1. Introduction

Understanding the interactions between millennial-scale variability and longer-term (orbital timescale) changes in climate is critical for explaining the non-linear relationship between periodic variations in Earth's orbit around the Sun and the shape and magnitude of glacial cycles within the so-called 100 kyr world (following the Mid Pleistocene Transition, MPT, 1.2–0.7 Ma) (Imbrie et al., 1993). For example, a range of studies have argued for the importance of millennial variability in the process of glacial termination (the end of a glacial cycle) (Barker & Knorr, 2021; Broecker & Denton, 1989; Cheng et al., 2009; Denton et al., 2010; Wolff et al., 2009). Here we focus on the transitions from interglacial to glacial (IG-G) conditions, which we contend also involve critical feedbacks between changing orbital configuration and millennial-scale variability. Specifically, we are interested in the pronounced oceanic cooling potentially associated with high amplitude oscillations of the Atlantic Meridional Overturning Circulation (AMOC) and (we suggest) the subsequent shift to a glacial mode of ocean stratification that results in the enhanced drawdown of atmospheric CO_2 characteristic of glacial periods within the mid to late Pleistocene.

The Last Glacial Maximum (LGM; 23–19 Ka) or Marine Isotope Stage 2 (MIS 2; 27–15 Ka) stands out as accommodating the largest ice sheets and lowest atmospheric CO_2 concentrations of the last glacial cycle (Figure 1). Yet an increasing number of studies highlight the extreme glacial nature of MIS 4 (70–60 Ka) in terms of surface temperatures (Barker & Diz, 2014; Jouzel et al., 2007; Kirst et al., 1999), glacier extent (Doughty et al., 2021; Schaefer et al., 2015) and deep ocean stratification (Curry, 1996; Hines et al., 2021; Thornalley et al., 2013). Of relevance to our study it has been suggested that enhanced deep ocean stratification during MIS 4 could have played an important role in lowering atmospheric CO_2 and ushering in glacial conditions at that time (Adkins, 2013; Barker & Diz, 2014; Bereiter et al., 2012; Ferrari et al., 2014; Hines et al., 2021). Recent work (S. Shackleton et al., 2021) also suggests that Mean Ocean Temperature (MOT) during MIS 4 (-2.7 ± 0.3°C relative to the Holocene) was comparable with the LGM (-2.6 ± 0.2, Bereiter et al., 2018, recently updated to

10.1029/2023PA004690

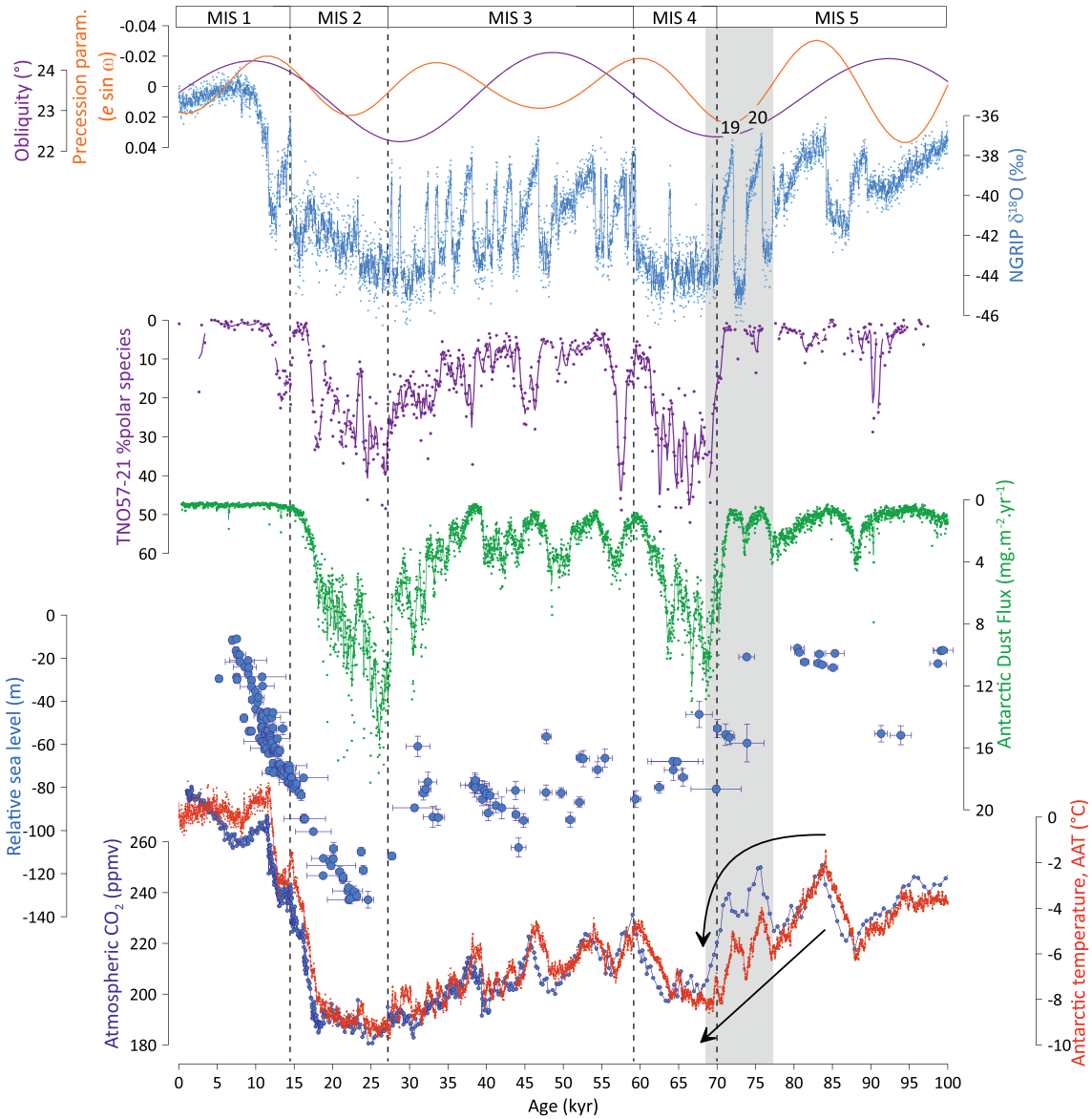

Figure 1. Climatic decoupling across the Marine Isotope Stage (MIS) 5/4 transition. From top to bottom: Uppermost curves show orbital parameters (Berger & Loutre, 1991); MIS 5/4 occurred when northern summers were relatively cool. NGRIP $\delta^{18}O$ (a proxy for Greenland temperature (NGRIP_members, 2004)) records two large amplitude DO oscillations (DO19 and 20) during the transition. Records of %polar planktic foraminifera from SE Atlantic site TNO57-21 (Barker & Diz, 2014) and dust accumulation in the EDC ice core (Lambert et al., 2012) highlight the delayed and abrupt descent into full glacial conditions at the onset of MIS 4. The record of sea level from fossil coral terraces (Thompson & Goldstein, 2006) also suggests a relatively rapid period of ice growth associated with this interval. Lowermost curves highlight the decoupling of Antarctic Temperature (AAT, red curve) from atmospheric CO_2 (blue curve), a result (we argue) of enhanced Antarctic (and mean ocean) cooling associated with DO19 and 20 and the delayed development of full glacial conditions. Vertical gray box encompasses DO19 and 20 and the climatic decoupling referred to throughout the text.

−2.1 ± 0.7°C (Pöppelmeier et al., 2023)). The transition from MIS 5 to MIS 4 occurred when northern summers were relatively cool (a function of low obliquity and positive precession parameter, meaning northern hemisphere summers coincided with aphelion; Figure 1), but unlike the gradual (~10 kyr) changes in Earth's orbital geometry, the final descent into MIS 4 was abrupt (≤3 kyr; Barker & Diz, 2014; Cutler et al., 2003; Woillard, 1979) and involved extreme oscillations in ocean and atmospheric circulation patterns (Dansgaard-Oeschger, DO events 19 and 20; Figures 1 and 2; Table S1 in Supporting Information S1).

Here we will argue that these oscillations were not merely a passive feature of the MIS 5/4 transition but played an active role in the development of glacial conditions. Specifically, we suggest that the very large amplitude of

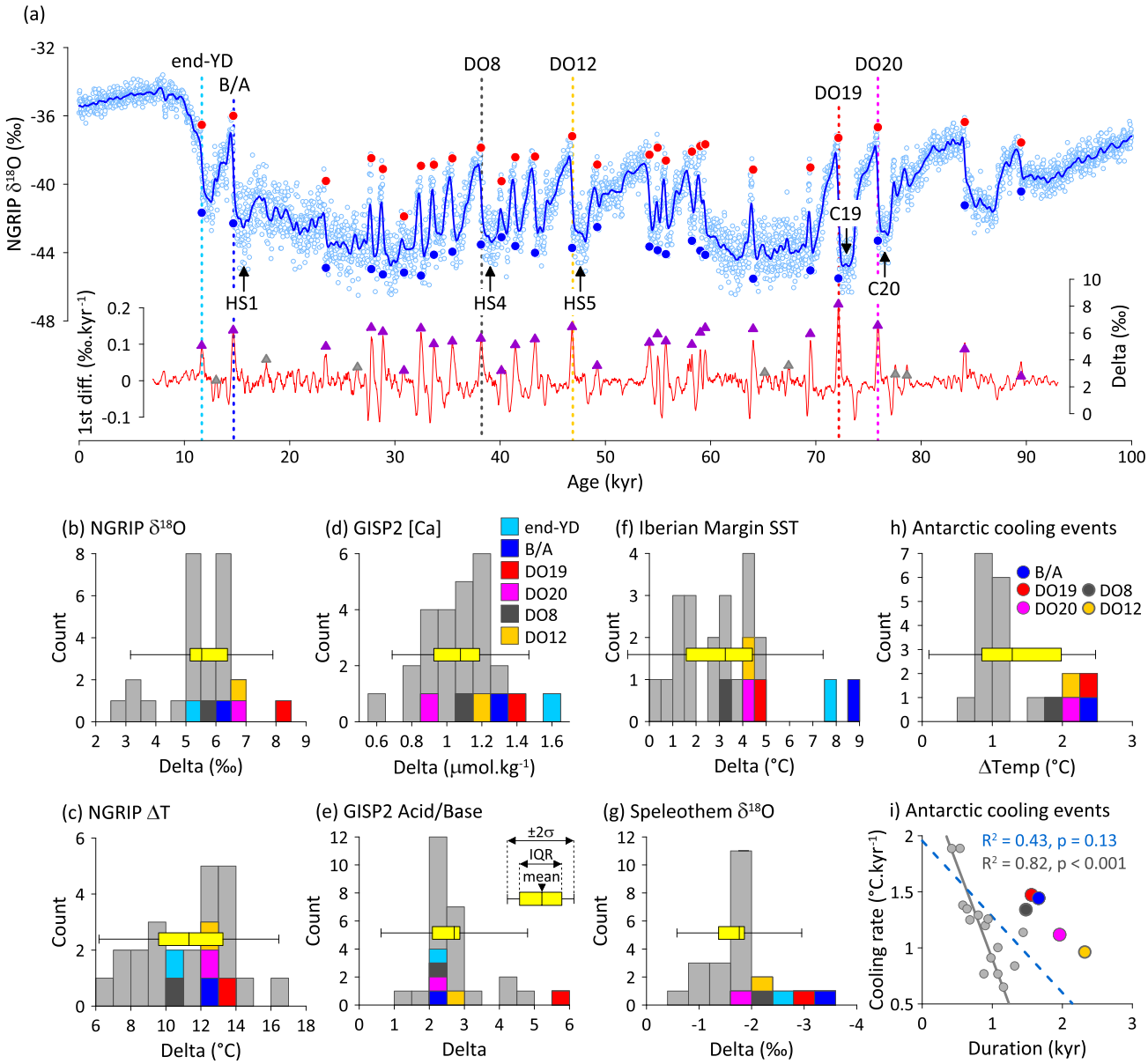

Figure 2. (a) Abrupt climate variability over the past 100 kyr recorded by Greenland ice core $\delta^{18}O$ (NGRIP_members, 2004), with individual stadial-interstadial warming transitions quantified using the algorithm described in methods. Briefly, the record is smoothed (blue curve) and differentiated (red curve) before individual peaks are selected. Maximum (red circles) and minimum (blue circles) values are then selected (from the raw data) from a time window (in this case ±0.3 kyr) either side of the identified peak. The max and min values are the average of the three highest and lowest values found (or fewer if less than 3 values are present). Delta values (purple triangles) represent the difference between max and min (those not related to canonical Greenland events (Rasmussen et al., 2014) are rejected, gray triangles). Prominent warming (DO) events are labeled. HS1, 4, 5 are Heinrich Stadials containing Heinrich Events 1, 4, 5. C19 and 20 are stadial events preceding DO19 and 20 respectively (Table S1 in Supporting Information S1) (b–g): Histograms of abrupt stadial-interstadial transitions from 6 records covering the last 100 kyr. In each case Delta represents the difference between max and min as shown in (a) (each record was treated separately, see Figure S1 in Supporting Information S1). In each case the yellow box represents the interquartile range, with the whiskers extending to two standard deviations either side of the mean (central line). Different colors represent named warming events. (h) Magnitude of Antarctic cooling (after removal of orbital trend) during Greenland interstadials (the record of AAT_hi is smoothed by 0.4 kyr in this case, see Section 2.1). (i) Cooling rate versus duration of events shown in (h). Cooling rates across DO19 and 20 are higher than the linear trend defined by all events (blue dashed line). Also included is a linear fit to all events ≤1.3 kyr in duration (gray line; see also Figures S2 and S3 in Supporting Information S1).

DO variability across MIS 5/4 acted to accelerate cooling across Antarctica (and throughout the global ocean, as evidenced by the record of MOT (S. Shackleton et al., 2021); Figure 3) through meridional heat flux adjustments associated with changes in the AMOC (for which we use the generic and intuitive term 'heat piracy'; Crowley, 1992; Pedro et al., 2018) in combination with the production of colder North Atlantic Deep Water

10.1029/2023PA004690

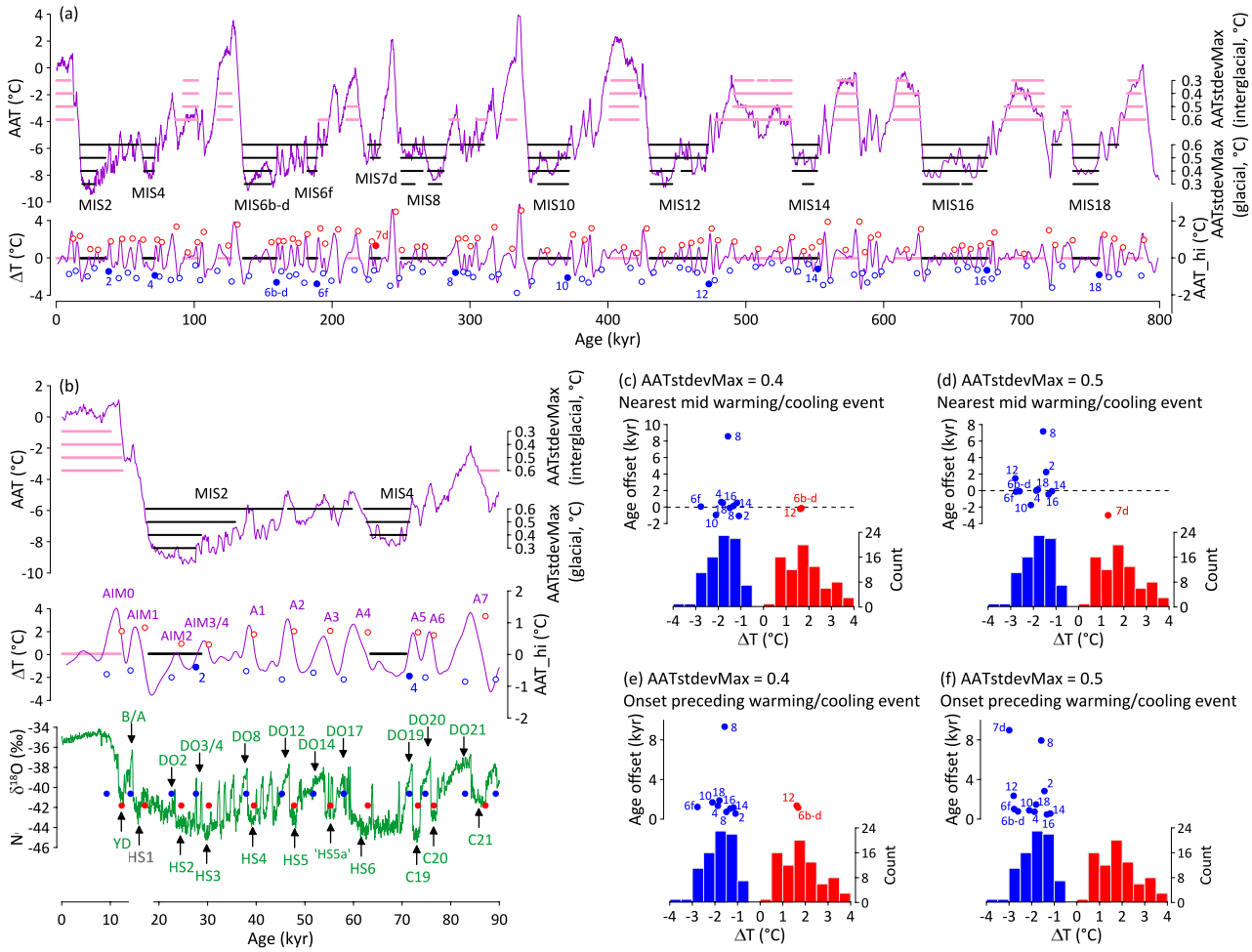

Figure 3. Extreme millennial-scale cooling precedes onset of glacial stability. (a) Upper: Stable intervals are identified in the Antarctic temperature record (AAT; Parrenin et al., 2013) using a maximum threshold of the standard deviation of AAT (AATstdevMax) over a 7 kyr period. Glacial versus interglacial periods of stability are defined according to whether they begin and end with AAT greater than (for interglacials, pink horizonal bars) or less than (glacials, black bars) −4.7°C (the mean of AAT over 800 kyr). Different thresholds of AATstdevMax imply longer or shorter intervals of stability. We suggest that AATstdevMax = 0.4 or 0.5 gives the most reasonable result (AATstdevMax = 0.3 excludes Marine Isotope Stage (MIS) 4 while AATstdevMax = 0.6 includes MIS 3). (a) Lower: The record of AAT_hi is smoothed by 1.4 kyr (purple curve) and differentiated before extreme minima and maxima are selected. ΔT values for warming (red symbols) and cooling (blue symbols) are then calculated from the raw stack using the same method as described in Section 2.1. Filled red and blue symbols are the closest warming/cooling events to the onset of glacial stability using AATstdevMax = 0.5 (results same as part d) and labeled according to their respective glacial MIS identifier. (b) Zoom-in on part (a) over past 90 kyr with Greenland $\delta^{18}O$ record (NGRIP_members, 2004) added for context. AATstdevMax = 0.4 (results same as part c). Major Antarctic Isotope Maxima and Antarctic Warming events (A1-7) are labeled, as are major Greenland stadials (Heinrich Stadial events) and HDO interstadials (see Table S1 in Supporting Information S1). Red and blue symbols overlaying Greenland record are the major Antarctic warming/cooling events selected by the algorithm, which are associated with prominent Greenland stadial/interstadial periods. (c–f) Major warming (red) and cooling (blue) events that precede the onset of glacial stability over past 800 kyr using values of AATstdevMax and selection method identified (numbered according to their respective MIS event; see Section 2.2 for description of selection methods). Histograms represent all major warming/cooling events selected over the past 800 kyr that is, equal to or larger than the major events highlighted in part (b). Total number of events of each type = 81. Age Offset is difference between age of event (mid-point in c and d, onset in e and f) and onset of glacial stability. See also results for AATstdevMax = 0.3 and 0.6 in Figure S4 in Supporting Information S1.

(NADW) throughout stadials and interstadials alike, as a consequence of orbital configuration. Meanwhile, other key components of the climate system, including atmospheric CO_2 and dustiness, sea surface temperature and ice volume were delayed on their path toward a glacial state, becoming "decoupled" from the cooling trend experienced by Antarctica (Figure 1). We suggest that once ocean cooling had progressed sufficiently, a change in deep water stratification (via an increase in the relative volume and or salinity of southern-sourced deep waters, SSW) became inevitable and the transition to full glacial conditions could rapidly ensue. Thus, we envisage that

enhanced millennial variability across MIS 5/4 played a role both in the trajectory and ultimately the magnitude of glacial development.

We extend our argument to include all interglacial-glacial (IG-G) transitions within the 100 kyr world, but not before. Our conclusions are based on new analyses of records spanning the last IG-G transition (MIS 5/4) together with longer records covering IG-G transitions over the past 800 kyr and beyond. Our study highlights the need for new reconstructions of deep ocean temperature, global ice volume and AMOC variability that can be used to test the hypotheses introduced here.

2. Materials and Methods

All analyses presented here were performed on previously published data sets, available from publicly accessible databases or from the authors themselves. In the following sections we describe the individual analyses used to generate the figures underlying our arguments.

2.1. Quantification of DO Transitions and Interstadials of the Past 100 kyr

In Figure 2 we use high resolution records representing key climatic variables to quantify the magnitude of environmental change across DO events 19 and 20 as compared with other events of the last 100 kyr (see also Figures S1–S3 in Supporting Information S1). To identify DO transitions (from stadial to interstadial conditions) each record was smoothed and differentiated and individual peaks in the rate of change (representing abrupt DO transitions) were then selected using the "islocalmax" function in MATLAB. Minimum and maximum values (representing conditions before and after each transition) were then selected from the raw data from a time window centered on the identified peak (±0.3 kyr for ice core records and ±0.8 kyr for Iberian Margin SST and speleothem records, to account for their generally lower resolution). Maximum and minimum values are the average of the 3 highest and lowest values found (or fewer if less than 3 values were present; Figure 2a). Delta values were then calculated as the difference between maxima and minima (those not related to canonical Greenland events (Rasmussen et al., 2014) were rejected). Delta values are plotted as histograms in Figures 2b–2g.

We also quantified the magnitude and rate of cooling across Antarctica during interstadial periods as defined in Greenland (Figures 2h and 2i; Figures S2, S3, and Table S1 in Supporting Information S1). For this we used the composite record of Antarctic temperature (AAT) based on a stack of 5 synchronized ice cores as described by Parrenin et al. (2013). We acknowledge that the regression slope for the isotopic composition of ice versus temperature is likely to vary over time and that changes in the AAT stack probably overestimate actual temperature changes (Buizert et al., 2021). However, the stack represents an average over a wide area, and we believe this compensates for its lack of absolute accuracy. The following calculations were performed both with and without removal of orbital timescale variability from AAT (by subtracting a 7 kyr smooth to give AAT_hi). To identify intervals of (interstadial) cooling the AAT record was smoothed and differentiated (to give AAT') and prominent minima selected using a threshold set to isolate only those minima associated with canonical events in Greenland (Rasmussen et al., 2014). The duration of cooling was defined as the interval of AAT' with a rate <0 encompassing each minimum. High (start) and low (end) values of AAT were then calculated from the raw (unsmoothed) stack as the average value across a 300-year window centered on the start and end of the cooling interval. The temperature difference (ΔTemp = high minus low) and rate of change (ΔTemp/duration) were then calculated. The calculated rates of change are highly dependent on the smoothing window employed before differentiating because of its effect on the duration of events (the duration of shorter events tends to be overestimated and the rate underestimated as the smoothing window is increased; Figures S2 and S3 in Supporting Information S1). Nevertheless, we find a systematic and negative relationship between cooling rate and duration for a range of smoothing windows. We also note that the rates of cooling obtained for DO interstadials 19 and 20 (using both AAT and AAT_hi) systematically lie above the relationship for all events of the last 100 kyr.

2.2. Rate of Change of Antarctic Temperature Prior to Onset of Glacial Stability

In Figure 3 we extend the previous analysis of AAT_hi to assess the timing of major warming and cooling events relative to the onset of glacial stability (see main text Section 3.2). Intervals of relative stability are defined as times when the standard deviation of AAT is lower than a stated threshold for at least 7 kyr (a range of thresholds

were assessed; Figure 3, Figure S4 in Supporting Information S1). In this way we are able to identify periods of stability associated with all major glacial (and interglacial) intervals over the past 800 kyr. Next, we wish to identify major warming/cooling events in AAT_hi. We do this by hunting for large peaks and troughs in AAT_hi', in a similar manner to our analysis of events over the past 100 kyr, but this time we are only interested in major events for example, the major Antarctic warming events described in earlier studies (Blunier & Brook, 2001). Significantly, the events identified by our algorithm (using a smoothing of 1.4 kyr) are precisely those associated with HDO events in the North Atlantic (i.e., oscillations between the extreme Heinrich stadials (HSs) and their subsequent interstadials). In addition, the algorithm picks warming/cooling events associated with DO19-21, which correspond to Antarctic warming events A5-7 as labeled by Blunier and Brook (2001) (Figure 3). Finally we determine which of the major warming/cooling events identified lead to periods of glacial stability. We do this in two ways, first we look for the major event whose mid-point is closest to the onset of glacial stability. Second, we start at the onset of glacial stability and look backwards in time for the onset of the previous major event. The two approaches give comparable results (Figure 3, Figure S4 in Supporting Information S1).

2.3. Deep-Sea Density Calculations

In Figure S5 in Supporting Information S1 we show recent results of MOT derived from noble gas measurements in glacial ice (Bereiter et al., 2018; S. Shackleton et al., 2020, 2021), which we combine with a stacked record of AAT (Parrenin et al., 2013) to derive an estimate of MOT spanning the last 800 kyr. Uncertainties in the calibration of MOT versus AAT were estimated using a Deming regression method (Browaeys, 2023). Here, the best slope and intercept are computed by minimizing the chi-square estimation using errors on both x and y. Data points are simulated using a Monte Carlo method (3,000 loops) to obtain uncertainties on the fitted parameters. Errors in MOT are taken from the original sources (mean error = ±0.3°C; although we note a recent estimate for the LGM increases this uncertainty to ±0.7°C, Pöppelmeier et al., 2023). We apply a constant error of ±0.5°C to the AAT stack. Uncertainties in the calibration are propagated through to density estimates in Figure S5 in Supporting Information S1.

In Figure 4 density calculations were made using the equation of state for seawater given by Gill (1983), implemented in a MATLAB routine by Ruiz-Martinez (2023). Mass balance considerations for temperature and salinity are described in the main text (Section 3.3.1).

2.4. Multiple Timeseries Analysis of the Past 800 kyr

In Figures 5–7, timeseries of "primary parameters", including ice core properties (AAT, Jouzel et al., 2007; Parrenin et al., 2013); atmospheric CO_2 (Bereiter et al., 2015; Nehrbass-Ahles et al., 2020) and Antarctic dust accumulation (Lambert et al., 2012), benthic $\delta^{18}O$ (the LR04 stack, Lisiecki & Raymo, 2005), Iberian Margin Sea Surface Temperature (IM SST, Martrat et al., 2007; Rodrigues et al., 2017) and NE Atlantic surface temperature (%Neogloboquadrina pachyderma from ODP Site 983, %NPS, Barker et al., 2019) are co-analyzed to allow assessment of their respective offsets through time (Figure 5). They were also compared with calculated orbital parameters (obliquity and precession, Berger & Loutre, 1991) and the records of Ice Rafted Debris (IRD) accumulation and Millennial Power from ODP Site 983 (calculated as the Hilbert transform of the 0.5–7 kyr Taner bandpass filtered %NPS record from this site, Barker & Knorr, 2021).

All timeseries span the past 800 kyr. In all cases we utilized previously published age models: AICC2012 (Bazin et al., 2013; Veres et al., 2012) for the ice core records and those from ODP 983, the LR04 age model (Lisiecki & Raymo, 2005) for benthic $\delta^{18}O$ and a combined approach for IM SST (Martrat et al., 2007; Rodrigues et al., 2017). The age model for the CO_2 record was slightly modified from AICC2012, with gas-ice depth differences (Δdepth) along the EDC ice core being determined by alignment of CH_4 with deuterium isotope maxima (Barker et al., 2019; Parrenin et al., 2012).

Individual timeseries were resampled onto a common timescale by binning data into 200 yr intervals (a comparison using 1 kyr intervals is shown in Figure S6 in Supporting Information S1), which is commensurate with the high sampling rates of ice core analyses and material from ODP Site 983. This allows cross-plotting of multiple timeseries (e.g., lowermost panels of Figure 7a–7f) but may bias individual data sets within the time domain for example, if accumulation rates are lower during certain intervals (during which a lower proportion of bins will be populated). Empty bins were therefore populated by linear interpolation for even representation in the

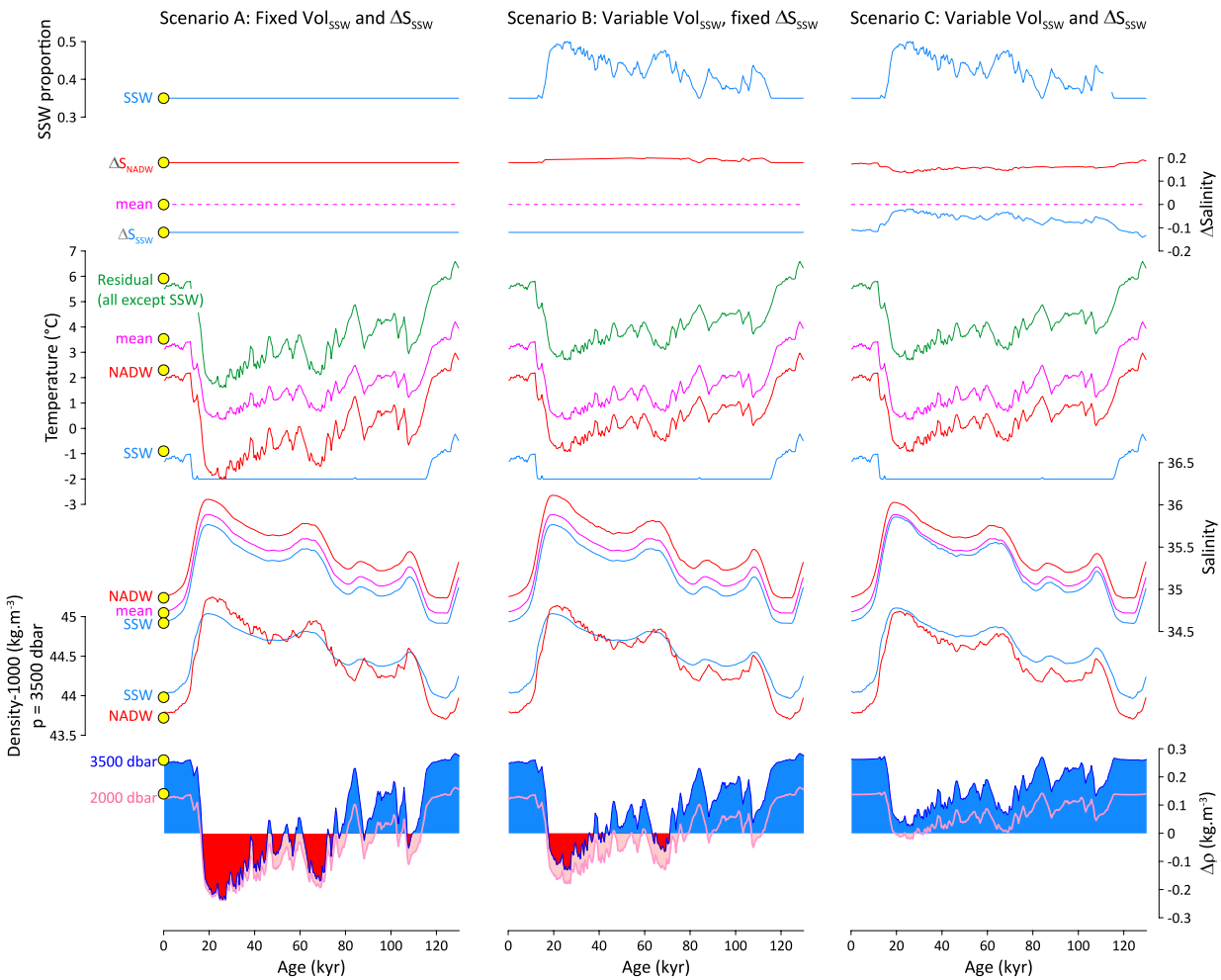

Figure 4. Ocean density calculations for the three scenarios described in Section 3.3.1. In each case "mean" represents the mean ocean, SSW is southern-sourced deep water, NADW is northern deep water. "Residual" is the whole ocean minus SSW. "SSW proportion" (Vol_{SSW}) is the relative volume of SSW within the whole ocean (modern value is 35%). ΔSalinity is the difference in Salinity from the mean ocean. $\Delta\rho$ is the density difference between SSW and NADW. Yellow circles represent modern values. Red (pink) shaded areas represent a potential density paradox at 3,500 (2,000) dbar pressure. See Figure S5 in Supporting Information S1 for estimated uncertainty on $\Delta\rho$. See Figure S9 in Supporting Information S1 for additional scenarios mentioned in the text.

time domain, to allow construction of histograms and for calculating mean values of one timeseries across the full range of another. Histogram bin widths were determined by dividing the total range of each parameter by a constant (a comparison using 10 and 20 bins is shown in Figure S6 in Supporting Information S1). Mean IRD accumulation and mean Millennial Power at ODP Site 983 (Figures 7a–7f top two rows) were calculated by binning and averaging these parameters according to the ranges of each primary parameter. The "sweet spot" of millennial activity for each parameter (blue vertical bars in Figure 7) is determined as those bins with Mean Millennial Power greater than a given proportion of the maximum Mean Millennial Power for each parameter (80% is used in Figure 7 but this can be reduced when using a smaller number of bins, Figure S6 in Supporting Information S1).

Following interpolation, all timeseries were normalized to have a mean of zero and standard deviation equal to 1. Offsets between individual timeseries and AAT were then calculated and further binned according to the full range of AAT, Millennial Power, obliquity, and precession (Figures 6 and 7g). To identify intervals where the offset between (normalized) CO_2 and AAT exceeded a threshold (vertical gray boxes in Figure 5) the calculated record of CO_2-AAT was smoothed (5 kyr running mean) and detrended (subtraction of 200 kyr running mean) to account for possible temporal biases in the preservation and/or measurement of either parameter (e.g., differences in extraction methods used to measure CO_2 can give rise to significant offsets in deeper parts of the ice core (Bereiter et al., 2015)).

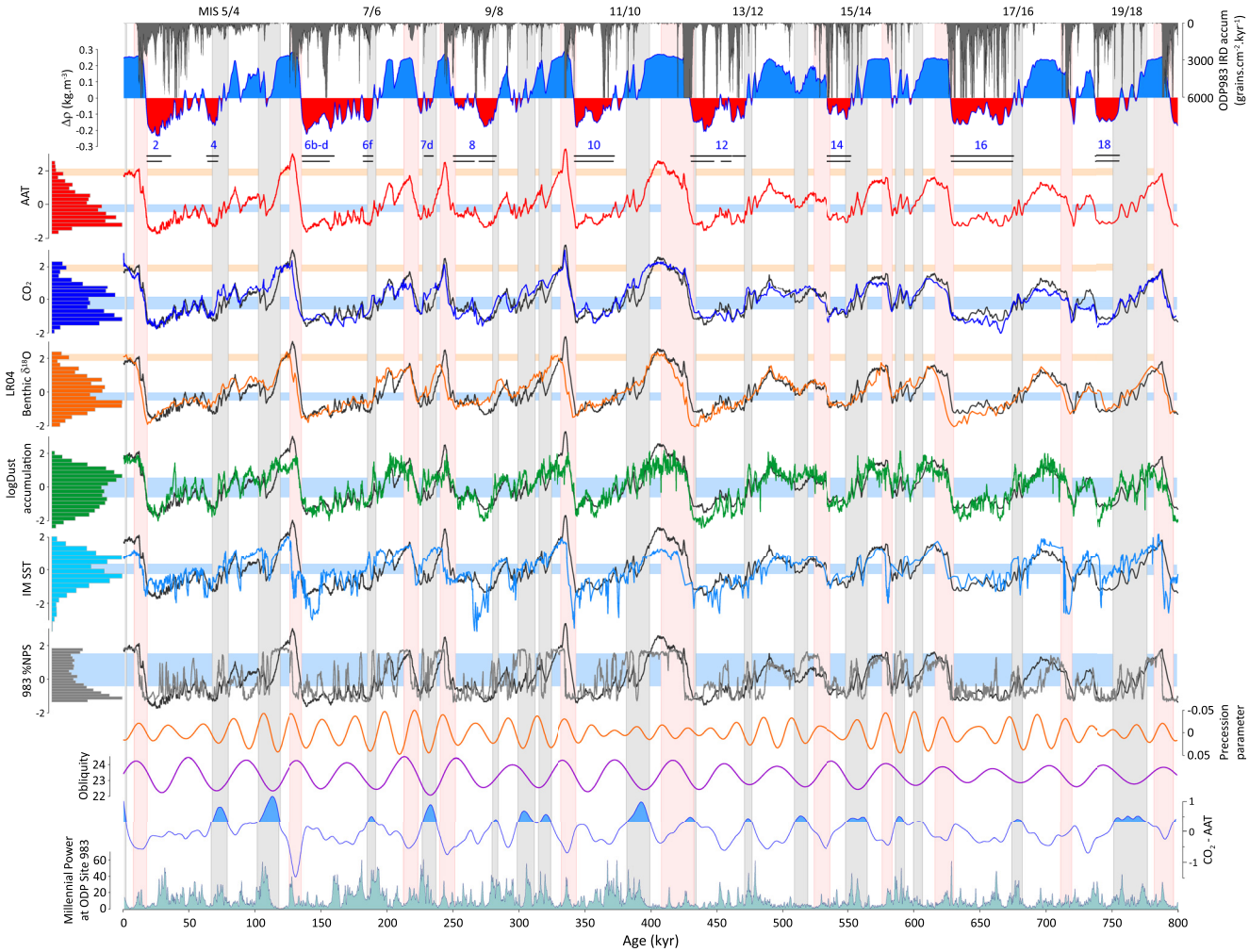

Figure 5. Decoupling of CO_2 (as well as benthic $\delta^{18}O$, atmospheric dustiness and North Atlantic SST) is a systematic feature of glacial development and gives rise to the appearance of bimodality. All records with histograms are normalized to have mean = 0 and stdev = 1. Record of Antarctic temperature (AAT) is plotted in black along with all other records to highlight intervals of decoupling. Records of Ice Rafted Debris accumulation and millennial-power from ODP 983 and calculated $\Delta\rho$ (SSW-NADW) are shown for reference, as are intervals of glacial stability from Figure 3 using AATstdevMax = 0.4 (lower) and 0.5 (upper) black bars. Vertical gray boxes are intervals of maximum decoupling between CO_2 and AAT (CO_2-AAT > 0.3, filled region of second to bottom curve). Horizontal blue boxes are maxima in millennial activity at Site 983 associated with each parameter as derived from the binning analysis shown in Figure 7. Vertical pink boxes are termination intervals, excluded from the histograms on the left-hand side. Note that the blue and gray boxes intersect during the transitions to glacial conditions. These transitions are also marked by a local minimum in the histograms of each parameter (except AAT). Horizonal orange boxes represent the second decoupling maximum shown in Figure 7.

3. Results and Discussion

3.1. Extreme Ocean/Climate Oscillations Across the MIS 5/4 Transition

Abrupt climate variability, as first observed within ice core records from Greenland (Figures 1 and 2), is now known to be a pervasive feature of the Pleistocene, with most archives pointing to enhanced millennial-scale activity (or Millennial Power) associated with intermediate climate states and the transitions between states (Barker et al., 2019; Hodell et al., 2023; Kawamura et al., 2017; Lambert et al., 2012; McManus et al., 1999). Many studies have also highlighted a direct link between so-called DO oscillations (abrupt transitions between stadial and interstadial conditions) and changes in circulation within the Atlantic basin, specifically the AMOC (Henry et al., 2016; Kissel et al., 2008; McManus et al., 2004). Notably, AMOC changes during the so-called HS events of MIS 3 and the last deglaciation (associated with massive iceberg discharge events across the North Atlantic; Heinrich Events) and the subsequent transitions to post-Heinrich interstadials (HDO) are thought to have been significantly more extreme than those corresponding to regular non-HDO oscillations (Barker et al., 2010; Henry et al., 2016). In this study we are interested in two very large DO oscillations that occurred during the transition

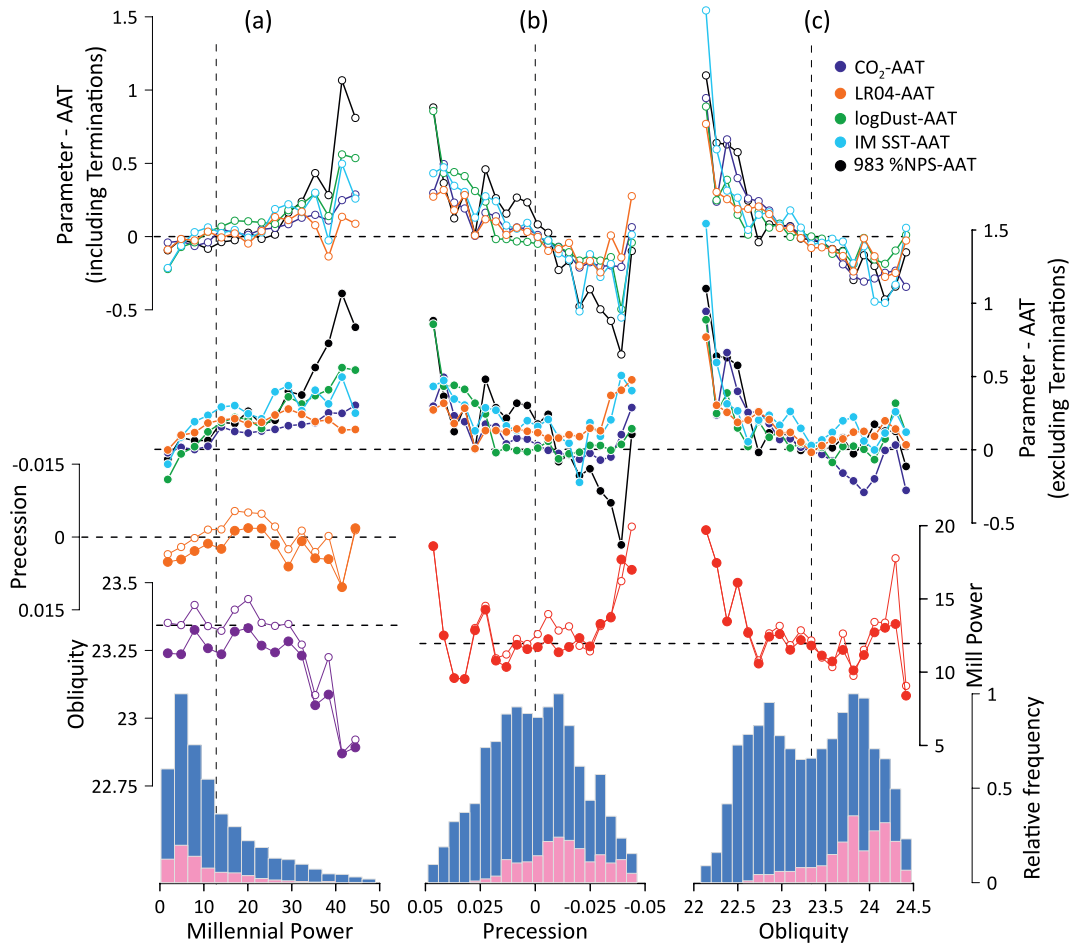

Figure 6. Relationships between climatic decoupling versus orbital parameters and millennial activity over past 800 kyr. (a–c) Upper two rows show extent of decoupling (parameter minus Antarctic temperature, AAT) versus Millennial Power, precession, and obliquity respectively. Top row includes termination intervals, second row excludes terminations. In part (a) precession and obliquity are also binned according to Millennial Power (hollow symbols represent all data, solid symbols exclude terminations). In parts (b, c) Millennial Power is binned according to precession and obliquity respectively. Lowermost histograms represent the temporal distributions of Millennial Power, precession, and obliquity over past 800 kyr (pink areas represent glacial terminations). Dashed lines indicate mean values in each case.

from MIS 5a to 4 (DO 19 and 20; Figures 1 and 2). These events are also thought to have involved perturbations of the AMOC (Böhm et al., 2015; Keigwin et al., 1994; Piotrowski et al., 2005; Thornalley et al., 2013). For example, reconstructed changes in the vertical structure of the NW Atlantic Deep Western Boundary Current (DWBC; a key component of the wider AMOC) suggest repeated shoaling and deepening of the DWBC (and by extension the AMOC) associated with stadial/interstadial transitions across DO19 and 20 (Thornalley et al., 2013) (Figure S7 in Supporting Information S1).

Here we wish to show that DO19 and 20 were very large events in terms of their impact on the ocean/atmosphere system, having a similar magnitude to the HS/HDO oscillations of MIS 3. However, existing reconstructions of AMOC variability are not highly resolved enough (temporally) to allow quantitative comparison of the magnitude of DO19 (and 20) with other events of the past 100 kyr. On the other hand, past abrupt shifts in ocean circulation were associated with equivalent changes in many other parts of the ocean/atmosphere system, some of which are recorded at high resolution in a range of climate archives. Here we focus on mid to high latitude temperature indicators, together with proxies for large scale atmospheric circulation patterns including the Asian monsoon (Figure 2, Figures S1–S3 in Supporting Information S1).

Records of $\delta^{18}O$ from the ice phase of Greenland ice cores (e.g., NGRIP; Figure 2a) reflect (to first order) variations in the temperature of local precipitation (NGRIP_members, 2004) and reveal a very large change

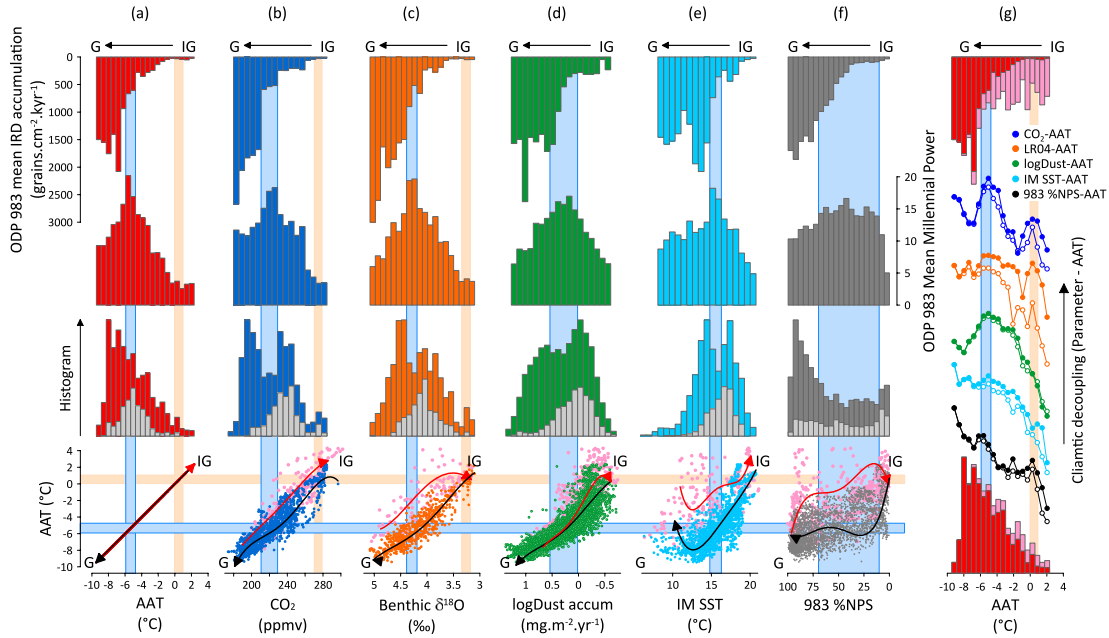

Figure 7. Binning analysis of key climatic variables for the past 800 kyr (excluding terminations). Panels (a–f) from top to bottom: Mean Ice Rafted Debris (IRD) accumulation and millennial-scale activity at ODP Site 983, binned according to the variables listed along the bottom. Vertical blues boxes highlight maxima in millennial activity (the "sweet spot") associated with each variable. Histograms of each variable reveal local minima (except for Antarctic temperature, AAT) aligned with the maximum in millennial activity. Gray subsets of each histogram are those intervals associated with maximum decoupling between CO_2 and AAT (as shown in Figure 5). In most cases (not AAT) these are associated with a "sub-glacial" mode. Glacial modes are aligned with maximum ice rafting at Site 983. Cross-plots (lowermost panels) between each variable and AAT reveal non-linear progression from interglacial to glacial conditions (IG-G; symbols colored according to each parameter) and back (G-IG; pink symbols in each case). Curved arrows are fourth order polynomial fits to the data for the last glacial cycle only (black arrows are IG-G, red are G-IG). Horizonal blue box is same as vertical box for AAT. Panel (g) Top: mean IRD accum at Site 983 binned according to the IG-G (red) and termination (pink) portions of the full 800 kyr AAT data set. Bottom: Histogram of AAT for the IG-G (red) and termination (pink) portions of the record. Colored curves are the difference between selected variables and AAT, binned according to AAT. Hollow symbols represent all data, solid symbols exclude terminations. Vertical blue box is the same as that in panel (a). This aligns with a local maximum in difference from AAT for each variable. A second decoupling maximum is highlighted by the orange boxes. In all cases (a–g) resampling bin width is 200 yr (see Section 2). Empty bins are populated by interpolation except for cross-plots where empty bins are left unpopulated.

associated with DO19 as compared with other events of the past 100 kyr (beyond 2 standard deviations, $>2\sigma$, from the mean; Figure 2b). The large magnitude of high latitude warming associated with DO19 is confirmed by nitrogen isotopes ($\delta^{15}N$) measured within the gas phase of the same ice core (Kindler et al., 2014) (Figure 2c). On the other hand, it should be acknowledged that Greenland temperature records are rather insensitive to the very cold conditions associated with Heinrich Events (massive ice rafting events), which affected North Atlantic sea surface temperatures much more strongly (Davtian & Bard, 2023; Li et al., 2005; Martin et al., 2023; Pedro et al., 2022; N. J. Shackleton et al., 2000). With this in mind we analyze a record of SST from the Iberian Margin recently published by Davtian and Bard (2023) (Figure 2f). The magnitude of warming associated with DO19 at this site is within the upper quartile of all events of the past 100 kyr (including those following Heinrich events; DO8 and 12 are highlighted) and is exceeded only by the deglacial Bølling/Allerød (B/A) and end-Younger Dryas (end-YD) events.

Variations in atmospheric dust loading over Greenland (recorded by the concentration of e.g., Ca within Greenland ice (Mayewski et al., 1997)) reflect changes in dust availability across the source region (thought to be eastern Asia, Biscaye et al., 1997) and its uplift and transport to higher latitudes (Barker & Knorr, 2007; Fuhrer et al., 1999). Within the Greenland dust record the onset of DO19 stands out as a prominent transition as compared with other events of the last 100 kyr (second largest event; Figure 2d) and this transition is particularly large within the acid/base record of the GISP2 ice core ($>2\sigma$ from mean; Figure 2e) (Barker, 2005), which is primarily a function of $[Ca]/[SO_4]$ within the ice (Figure S1 in Supporting Information S1). A high ratio of [Ca] to $[SO_4]$ during the cold stadial preceding DO19 (C19; Table S1 in Supporting Information S1) implies that anomalous conditions at this time were not due to the super-eruption of the Toba volcano (which would produce a low ratio

of [Ca]/[SO_4] (Legrand et al., 1997)). Instead, relatively high [Ca]/[SO_4] ratios are thought to reflect a greater proportion of $CaCO_3$, relative to gypsum ($CaSO_4 \cdot 2H_2O$) within dust reaching Greenland, which could reflect either a much larger volume of uplifted dust (relative to the acidic compounds available to neutralize $CaCO_3$ within the atmosphere) or a shorter transit time between Asia and Greenland (Legrand et al., 1997). Either way, the transition from C19 to DO19 coincided with a very large change in atmospheric conditions.

Chinese speleothem $\delta^{18}O$ records (Cheng et al., 2016) also imply large amplitude variations in atmospheric circulation patterns across MIS 5/4 (Figure 2g). Abrupt events in the speleothem record, superimposed on longer-term changes driven by precession, occurred in parallel with DO oscillations over Greenland throughout the last 100 kyr (Wang et al., 2001) and are thought to reflect changes in Asian monsoon intensity. An alternative interpretation (Pausata et al., 2011) suggests that these records are more strongly influenced by changes in the Indian monsoon but for our purposes it is sufficient to conclude that DO19 involved a particularly large shift in atmospheric circulation patterns ($>2\sigma$ from mean for speleothem $\delta^{18}O$).

3.1.1. Southern End of the Bipolar Seesaw: Antarctic Cooling Across MIS 5/4

Finally, we employ the Antarctic temperature record (AAT and AAT_hi, see Section 2.2) to quantify the rate of Antarctic cooling associated with Greenland interstadials over the past 100 kyr (Figures 2h and 2i, Figures S2 and S3 in Supporting Information S1). The inverse relationship observed between rate of change of AAT and the temperature anomaly over Greenland (Barker et al., 2011; Stocker & Johnsen, 2003) reflects the meridional redistribution of heat associated with changes in the AMOC (Crowley, 1992; Pedro et al., 2018). Overall we observe a negative relationship between the duration of Antarctic cooling events and their rate of cooling (Figure 2i). To our knowledge this relationship has not been described previously but an equivalent observation has been made with respect to the duration of Greenland interstadials and their respective cooling rates (Barker et al., 2015; Schulz, 2002). Furthermore, we note that our calculated cooling rates for DO19 and 20 lie above any straightforward fit to the overall trend observed (Figures S2 and S3 in Supporting Information S1). Hence, we can state that the rate of Antarctic cooling associated with DO19 and 20 was greater than would be predicted from their duration alone. Our analysis highlights DO19 and 20 as particularly large cooling events across Antarctica ($>2\sigma$ from the mean; Figure 2h). In particular, we find that the magnitude and rate of cooling during DO19 and 20 were comparable with those interstadials following HS events of MIS 3 and the last deglaciation, which experienced pronounced weakening/strengthening of the AMOC (HS1/B-A, HS4/DO8, HS5/DO12; Henry et al., 2016; McManus et al., 2004). We suggest this implies a relatively strong mode or at least strong recovery of AMOC during DO19 and 20, which is in line with studies using various kinematic and tracer-based approaches that suggest a strong and/or deep mode of AMOC during these intervals (Böhm et al., 2015; Keigwin et al., 1994; Piotrowski et al., 2005; Thornalley et al., 2013) (Figure S7 in Supporting Information S1).

In summary, our analysis of events across the MIS 5/4 transition (Figure 2) suggests that DO19 and 20 involved very large amplitude shifts in ocean/atmospheric conditions, comparable with those associated with the HS/HDO events of MIS 3 and the last deglaciation. By analogy with those events, which involved extreme perturbations of the AMOC (relative to non-HDO oscillations; Barker et al., 2010; Henry et al., 2016; McManus et al., 2004) we suggest that DO19 and 20 also involved extreme oscillations in Atlantic Ocean circulation. Of course, there is no guarantee that the relationships between AMOC and other aspects of the climate system (e.g., monsoon strength or Antarctic warming/cooling), as reconstructed for MIS 3 and the last deglaciation, were the same during DO19 and 20. We must therefore remain somewhat speculative in this respect and await future AMOC reconstructions across MIS 5/4 and earlier IG-G transitions that will provide a test of our conjecture.

3.2. Extreme Antarctic Cooling Precedes the Onset of Glacial Stability

DO19 was the last large amplitude millennial-scale event before the onset of MIS 4 (Figure 1). Subsequent events during MIS 4 (e.g., DO19.1 and DO18) were shorter and less frequent than those of for example, MIS 3 (Figure 1, Figures S1–S3 in Supporting Information S1). The relatively subdued nature of millennial variability during full glacial (and interglacial) periods is well documented (Barker et al., 2019; Hodell et al., 2023; Kawamura et al., 2017; McManus et al., 1999), with previous studies suggesting that such relative quietude might be a consequence of increased ice sheet size (Sima et al., 2004; Zhang et al., 2014), enhanced ocean stratification (Barker et al., 2010; Lynch-Stieglitz et al., 2014), or a pre-weakened state of AMOC being less sensitive to for example, freshwater perturbations (Kawamura et al., 2017). Irrespective of the underlying reason, we can exploit

the fact that millennial-scale variability is subdued during full glacial periods to identify such intervals within the AAT record. Our objective here is to identify whether glacial periods are systematically preceded by major millennial-scale warming or cooling events, which would enable us to better constrain the mechanism leading to such conditions. Note we do not use a glacial definition based on a specific temperature threshold, because it seems rather obvious that cold episodes will be preceded by periods of cooling, not warming.

Following the procedure described in Section 2.2 and using a wide range of standard deviation thresholds, we find that glacial stability is consistently (>80% of instances) preceded (within 1–2 kyr) by periods of major cooling across Antarctica (Figure 3, Figure S4 in Supporting Information S1). Because these intervals are synonymous with those interstadials following the Heinrich events of MIS 3-2, we can state that periods of glacial stability are systematically preceded by major interstadial events which, we suggest, are associated with a strong mode of AMOC.

We believe this result has important implications. First, if the enhanced amplitude of millennial activity associated with intermediate climate states were simply a consequence of such conditions (e.g., Sima et al., 2004) and played no role in the transitions from interglacial to glacial state (e.g., as a feedback), then a priori there is no reason why the onset of glacial conditions should favor a preceding interval of interstadial or stadial type. Thus we suggest our result implies an active role of millennial-scale variability in the transition to a glacial state. Second, the fact that glacial onset is preceded so consistently by millennial-scale cooling across Antarctica suggests that it is the interstadial mode, associated with a strong mode of AMOC, that is (at least in part) responsible for the transition to a glacial state. Below we consider why this might be the case.

3.3. Cooling of the Deep Ocean Across MIS 5/4

Recent results from Taylor Glacier, Antarctica suggest rapid cooling (-0.41 ± 0.09°C kyr^{-1}) of the global ocean across DO19, to a temperature in line with estimates for the LGM (S. Shackleton et al., 2021) (Figure S5 in Supporting Information S1). Modeling studies demonstrate how large-scale changes in the AMOC can drive changes not only in AAT and that of SSW (Knorr et al., 2021) but also the wider ocean interior (Pedro et al., 2018) and ultimately the whole (mean) ocean (Galbraith et al., 2016). Our previous analyses highlighted the extreme magnitude of millennial variability across MIS 5/4, and we conclude therefore that an enhanced mode of AMOC associated with DO19 played an important role in deep ocean cooling at this time, as also suggested by S. Shackleton et al. (2021). DO variability across MIS 5/4 also occurred when obliquity was low and northern summers coincided with aphelion (Figure 1). This would have accentuated cooling across this interval by the formation of colder NADW under the influence of cooler northern hemisphere summers (Adkins, 2013; Barker & Diz, 2014).

On the other hand, as S. Shackleton et al. (2021) point out, since MOT was already ∼2°C lower than modern by the onset of DO19, the majority of mean ocean cooling following the penultimate deglaciation (Termination 2, T2) must have occurred during MIS 5. Furthermore, modern SSW (Antarctic Bottom Water, AABW, $T_{\mathrm{AABW}} = -0.9$°C, $S_{\mathrm{AABW}} = 34.6$, Johnson, 2008) is close to the freezing point of seawater ($T_{\mathrm{freeze}} \approx -2$°C) which probably means that SSW had already cooled to T_{freeze} well before the MIS 5/4 transition (Figure S5 in Supporting Information S1). The fact that SSW cannot cool by more than ∼1.1°C before reaching T_{freeze} has important implications for Atlantic water column stability if MOT cools to a substantially greater extent (cf. Knorr et al., 2021). All else being equal a decrease in MOT of 2.5°C (with respect to modern) would imply that the residual ocean (everything other than SSW) cooled by considerably more than 2.5°C (because of the limited cooling capacity of SSW; Figure 4). However, cooling modern NADW to −0.3°C (a decrease of 2.6°C) would make it equal in density to AABW at −2°C and a pressure of 3,500 dbar (≅3,500 m, the approximate depth of the modern boundary between NADW and AABW). Any further decrease in the temperature of NADW would make it denser than AABW (Figure 4), which in theory would allow it to replace SSW as the deepest water mass in the Atlantic basin.

However, evidence from water mass tracers such as δ^{13}C and Nd isotopes suggests that SSW maintained its position as the deepest Atlantic water mass throughout the last glacial cycle, including the LGM and MIS 4 (Curry, 1996; Curry & Oppo, 2005; Hines et al., 2021; Oppo et al., 2018; Piotrowski et al., 2008) with the possible exception of a particularly dense abyssal (5 km) water mass identified in the western North Atlantic, thought to have formed through brine rejection in the Labrador Sea (Keigwin & Swift, 2017). In fact the boundary between NADW and SSW may have shoaled by hundreds of meters during the LGM (previous estimates for the

glacial boundary between NADW and SSW range from >3,000 m up to 2,000 m; Curry & Oppo, 2005; Hines et al., 2021; Lynch-Stieglitz et al., 2007; Oppo et al., 2018) and may also have shoaled during MIS 4 (Curry, 1996; Thornalley et al., 2013), although this is debated (Pöppelmeier et al., 2021). At shallower depths the problem highlighted above becomes exacerbated because of the dependence of seawater thermal expansibility on pressure that is, the thermobaric effect (McDougall, 1987). Cooling NADW to −0.3°C at depths shallower than 3,500 m would make it denser than AABW at −2°C (at the same depth) if their respective salinities were maintained. Yet, according to the majority of evidence, the density of NADW never exceeded that of SSW, which means some other change must have occurred to maintain the density contrast between these two water masses. Adkins (2013) suggested that the production of colder NADW across MIS 5/4, as a consequence of cooler northern summers, could have promoted the generation of saltier AABW through a reduction in ice melt around Antarctica (Miller et al., 2012). This could have counteracted the effect of a reduced temperature gradient between AABW and NADW by altering their salinity contrast. Alternatively (or in addition) Bereiter et al. (2018) pointed out that increasing the relative volume of SSW in the global ocean (which would be implied by a glacial shoaling of the boundary between SSW and NADW) could also accommodate much of the reduction in MOT, thereby reducing the degree to which NADW might have cooled.

3.3.1. Implications of Extreme Cooling for the Relative Volume and Salinity of SSW

MOT data published previously encompass key periods and transitions over the last glacial cycle. These results demonstrate a quite remarkable relationship between MOT and AAT, as pointed out by S. Shackleton et al. (2021). Here we capitalize on this to produce a prediction for the evolution of MOT over the past 800 kyr using the AAT stack presented by Parrenin et al. (2013) (Figure S5 in Supporting Information S1). We acknowledge that our estimation is crude, and substantial uncertainty remains as to why variations in MOT are so well aligned with those in AAT and whether this covariation held during other periods (S. Shackleton et al., 2021). Furthermore variations in mean-ocean noble gas saturation (Pöppelmeier et al., 2023) and refinements in the fractionation corrections applied when calculating MOT (S. Shackleton et al., 2020) will likely mean current estimates of MOT will need revising in the future. Notwithstanding, our approach provides a first order estimate of MOT that allows us to test some of the basic ideas about changes in relative temperature, volume and salinity referred to above (Figure 4). In the following scenarios all water masses are assumed to cool (from their interglacial state) in parallel with the mean ocean until the temperature of SSW (T_{SSW}) reaches T_{freeze}. At this point the residual ocean (i.e., all water masses except SSW) cools at a rate required to accommodate the now constant temperature of SSW. NADW is assumed to cool in parallel with the residual ocean. Mean ocean salinity varies as a function of sea level as modeled by Bintanja et al. (2005).

In Scenario A (Figure 4) the relative volume of SSW (V_{SSW}) is kept fixed, as are the salinity offsets between SSW and NADW with respect to the mean ocean (ΔS_{SSW} and ΔS_{NADW} respectively). This demonstrates the "density paradox" alluded to above as the temperature gradient between NADW and SSW decreases until $\rho_{NADW} > \rho_{SSW}$. Notably this theoretical paradox occurs at around 70 ka, as MOT decreases rapidly into MIS 4 (see also Figure S5 in Supporting Information S1).

In Scenario B we allow V_{SSW} to increase as a linear function of decreasing MOT once T_{SSW} reaches T_{freeze}. We consider this to be a pragmatic solution to the problem of connecting the cooling signal observed across Antarctica with that of the mean ocean, which intuitively must involve processes within the Southern Ocean (possibly including the formation of SSW). Following Bereiter et al. (2018) we allow the proportion of SSW to increase from 35% (its current volume, Johnson, 2008) to a maximum of 50% as MOT reaches its minimum value (Figure 4). Note that this increase could be accommodated by adjustments outside of the Atlantic basin and does not necessarily require a significant shoaling of NADW. Increasing the proportion of SSW in this way effectively compensates for the loss of cooling capacity of SSW once it reaches T_{freeze} (so that the residual ocean trend remains parallel with the mean ocean) but is not sufficient to overcome a density paradox during the LGM or MIS 4, even at 3,500 m.

In Scenario C we additionally allow the relative salinity of SSW (ΔS_{SSW}) to increase as a linear function of decreasing T_{NADW} (which occurs in parallel with the residual ocean) to reflect the proposed influence of changing NADW temperature on the melting of continental ice around Antarctica and consequently the salinity of newly formed SSW (Adkins, 2013; Miller et al., 2012). Changes in ΔS_{SSW} are mirrored by the residual ocean (as required by mass balance) and hence ΔS_{NADW}. Our results suggest that a density paradox can be avoided (even at depths as shallow as 2,000 m) by increasing the relative volume of SSW to 50% and its salinity by 0.1 (the

maximum change in ΔS_{SSW} applied as T_{NADW} reaches its minimum value) relative to the mean ocean. Such an increase in S_{SSW} is within current estimates for the LGM salinity of SSW based on porewater studies (Adkins et al., 2002; Insua et al., 2014). In an additional scenario (D; Figure S9 in Supporting Information S1) we applied the same adjustment to S_{SSW} but without a simultaneous change in V_{SSW}.

We have made very simple assumptions about relative rates/extent of cooling and salinity gradients between water masses to highlight first order adjustments that could be made to avoid a density paradox in the deep Atlantic. A smaller reduction in the temperature gradient between NADW and SSW could also be achieved by allowing some other part of the global ocean (e.g., the upper North Pacific) to cool more than the mean ocean, which would require less cooling of NADW. We have few absolute estimates of intermediate/deep Atlantic temperature across the last glacial cycle. Skinner et al. (2003) used paired benthic foraminiferal Mg/Ca and $\delta^{18}O$ measurements to reconstruct temperatures across the last deglaciation at 3,146 m in the NE Atlantic (Figure S8 in Supporting Information S1), and we note that these follow a trend broadly parallel to that of MOT. Estimates of bottom water temperature from the same site can be obtained directly from its record of benthic $\delta^{18}O$ (N. J. Shackleton et al., 2000) by subtracting the effect of ice volume and assuming the residual is controlled only by temperature (Adkins, 2013; Chappell & Shackleton, 1986). Although cruder, the estimates obtained in this way also suggest that the deep Atlantic may have cooled by a similar magnitude as the mean ocean during MIS 4 and 2 (Figure S8 in Supporting Information S1), which is in broad agreement with our calculations in Scenarios B and C, in which NADW cools in parallel with MOT. Clearly there is an urgent need to generate new records of deep ocean temperature across IG-G transitions to test these assumptions.

In scenarios A-C we assumed a constant salinity offset between NADW and the residual ocean (which equates to a constant offset between NADW and e.g., the Indo-Pacific), but this may also have varied through time. For example, net atmospheric moisture export from the Atlantic to Pacific basins (Weyl, 1968; Zaucker & Broecker, 1992) produces an evaporative regime in the modern Atlantic (Baumgarter & Reichel, 1975), resulting in a positive offset between S_{NADW} and the residual ocean (including e.g., the Indo-Pacific). In a further 3 scenarios (E-G, Figure S9 in Supporting Information S1) we therefore allow the salinity offset between NADW and the residual ocean to vary (by a factor of -1 to 2) in order to simulate hypothetical changes in the hydrological cycle. All else being equal a density paradox is still predicted at 3,500 m during MIS 4 even in the extreme hypothetical case where NADW becomes fresher than the mean ocean (Scenario G).

We suggest that our results highlight a critical role for millennial variability in glacial development across MIS 5/4 by promoting deep ocean cooling to an extent that can only have been accommodated by a change in deep ocean stratification through volume expansion and/or salinification of SSW. We note that it is possible that gradual changes (e.g., cooling of NADW by decreasing northern summer insolation) provided the main impetus for the shift to a glacial mode of stratification (e.g., Adkins, 2013) and that the amplified cooling associated with DO19 merely provided the final kick (e.g., Barker & Diz, 2014). However, it is also possible that the cumulative effect of DO19 and 20 drove a net cooling and densification of the deep ocean, without which a transition to glacial stratification could not have occurred. For example, the density of SSW formed during DO19 and 20 would have been enhanced by the combined effects of cooler precursor NADW (formed in response to reduced northern summer insolation) and the heat piracy associated with an enhanced mode of AMOC. They may also have been saltier, either as a result of reduced ice melt around Antarctica (Adkins, 2013; Miller et al., 2012) or by increased formation and export of sea ice as obliquity decreased (Otto-Bliesner et al., 2007; Shin et al., 2003; Zhang et al., 2013). In contrast, SSW formed during the intervening stadial events (C19 and 20, or GS-20 and 21 according to the INTIMATE nomenclature; Table S1 in Supporting Information S1) would have been warmer and relatively less dense, thanks to a reduction in heat piracy. This contrast in density would effectively mean a longer timescale for replacement of abyssal waters during a stadial mode compared with an interstadial. If this difference in timescale was of a similar magnitude to the duration of interstadial and stadial events themselves, it would lead (over multiple DO cycles) to a net build-up of interstadial-mode SSW in the abyssal ocean with concomitant cooling and densification of the deep ocean over and above that which might be possible by gradual changes in insolation alone.

3.4. Climatic Decoupling During the Transition to a Glacial State

In contrast to the net cooling experienced by AAT across DO19 and 20, other key climate parameters (n.b. atmospheric CO_2) were apparently delayed on their path toward glacial conditions and thus became decoupled from

AAT during this key interval of enhanced millennial activity (Figure 1). Previous explanations for the temporal offset between AAT and CO_2 at this time emphasize the importance of physical and biogeochemical processes in the coupled ocean-atmosphere system (Barker & Diz, 2014; Barnola et al., 1987; Menking et al., 2022) that might be complemented by additional contributions from solid Earth-climate feedbacks (Hasenclever et al., 2017; Köhler & Munhoven, 2020; Köhler et al., 2018) for example, depending on the magnitude and timing of sea level lowering across MIS 5/4. We have already suggested that the cooling trend of AAT across MIS 5/4 may have been influenced by millennial activity at this time, but the transient decoupling observed was also a function of the way in which CO_2 varied across the same interval, which can be considered in one or both of two ways:

1. if CO_2 had declined along with AAT across MIS 5/4 (as might be expected from the covariance of these two parameters at other times; Figure 1; Ahn & Brook, 2008; Parrenin et al., 2013) then no decoupling would have occurred.
2. if CO_2 had remained relatively high beyond the transition to MIS 4 then the period of decoupling would not have ended at that point.

With respect to (1) a first order prediction from orbital theory is that climate should have been transitioning toward a glacial state across MIS 5/4 as northern summer insolation decreased (Figure 1). The fact that CO_2 remained at a relatively high level throughout this period suggests to us that it was actively "held up" by some other agent and we suspect that DO oscillations 19 and 20 played an important role. For example, higher levels of CO_2 on a millennial timescale may occur in response to intense stadial conditions (e.g., Ahn & Brook, 2008) or on a centennial timescale with the subsequent transition to interstadial conditions (e.g., Marcott et al., 2014). Clearly though, more work is needed to explain why these effects were not undone for example, during DO20. With respect to (2) the abrupt drop of CO_2 into MIS 4 is thought to reflect an increase in the relative volume of SSW and or enhanced deep ocean stratification at that time (Adkins, 2013; Bereiter et al., 2012; Hines et al., 2021; Thornalley et al., 2013; Yu et al., 2016), which we also ascribe to the influence of pronounced millennial activity across MIS 5/4 (Section 3.3). Therefore, with respect to both (1) and (2), we suggest that enhanced millennial activity played an active role in the evolution of CO_2 across MIS 5/4 and therefore in its decoupling from and subsequent reunion with AAT across that interval.

3.4.1. Systematic Climatic Decoupling Over Past 800 kyr: A Result of Enhanced Millennial Power at Times of Low Obliquity

If we are correct that enhanced millennial activity during the MIS 5/4 transition played an active role in the development of glacial conditions, then we should expect to find evidence for similar interactions during earlier IG-G transitions. Fortunately, several records exist that enable us to investigate this. In Figure 5 we plot several of these records over the past 800 kyr. We include the predicted density contrast ($\Delta\rho$) between NADW and SSW (Figure 4), calculated without changes in the volume or salinity of SSW, to highlight periods where substantive changes in water column structure and deep ocean salinity would be required to maintain SSW as the deepest Atlantic water mass. We note that these tend to occur in parallel with periods of glacial stability (according to our definition) and increased ice rafting at NE Atlantic ODP Site 983 (Barker et al., 2019), highlighting the link between the deep ocean and land-based ice sheets on G-IG timescales. This is perhaps not surprising, given the observed link between MOT and AAT (Figure S5 in Supporting Information S1) but we also note that each interval of potential "density paradox" was preceded by a period of climatic decoupling (in this case quantified by the offset between CO_2 and AAT; gray vertical boxes in Figure 5). Furthermore many of these decoupling intervals coincided with periods of enhanced millennial power (in this case quantified by the Hilbert transform of the 0.5–7 kyr Taner bandpass filtered %NPS record from ODP Site 983), low obliquity and positive precession parameter (i.e., relatively cool northern hemisphere summers).

These relationships are quantified in Figure 6, where we plot the offsets between key climate parameters and AAT versus millennial power, obliquity, and precession over the past 800 kyr. We find that decoupling is greatest when millennial power is high, obliquity is low, and the precession parameter is positive, analogous to conditions across the MIS 5/4 transition. We also note that millennial power tends to be stronger when obliquity is low and likewise, obliquity tends to be low when millennial power is high. This contrasts slightly with the connection to precession, which if anything implies a link between negative precession parameter and higher millennial power. Furthermore, by excluding intervals associated with glacial termination (pink vertical boxes in Figure 5) we find that enhanced decoupling can also occur when the precession parameter is negative. We therefore conclude that periods of climate decoupling, which typically preceded intervals of deep ocean restructuring (as implied by

$\Delta\rho$) throughout the past 800 kyr, were a systematic biproduct of enhanced millennial power during intervals of cool northern summers, primarily as a function of low obliquity. Of course we expect exceptions to the average relationships shown in Figure 6. For example, during MIS 3 and 6, high millennial power was aligned with high obliquity. On the other hand, decoupling was not high during those intervals. In fact we suspect that IG-G transitions might be unique in the triplet of low obliquity, high millennial power and climatic decoupling.

Here we are most interested in the consequences of millennial-scale variations for the development of glacial conditions, but the cause of such variability is obviously an important consideration. In this respect it is apparent from our results that insolation must play some role (given the observed link between e.g., obliquity and millennial power; Figure 6). Previous studies have shown that millennial variability reaches its maximum power somewhere between full glacial and full interglacial conditions (Barker et al., 2019; Hodell et al., 2023; Kawamura et al., 2017; Lambert et al., 2012; McManus et al., 1999), possibly reflecting the dampening effects of large ice sheets during glacial maxima and high levels of CO_2 during interglacial periods (Galbraith & de Lavergne, 2019; Zhang et al., 2017), but also perhaps the degree of deep ocean stratification as alluded to earlier. The MIS 5/4 transition occurred when CO_2 had already decreased below interglacial values, and well before ice sheets had grown to their maximum size. Therefore it is possible that the combination of ice sheet size and CO_2 concentration became just favorable for the spontaneous occurrence of AMOC fluctuations at the MIS 5/4 transition. However, we do not know the precise history of ice volume across this interval and CO_2 had remained relatively constant for much of the preceding MIS 5 (Figure 5). Alternatively, it has been shown that subtle changes in obliquity or precession can directly trigger abrupt transitions in the AMOC when background conditions are favorable (i.e., within an intermediate climate) (Zhang et al., 2021). This possibility could explain why we find such a consistent relationship between the occurrence of enhanced millennial power and orbital configuration (Figure 6). Again though, we need new reconstructions of deep ocean temperature and ice volume across key transitions such as MIS 5/4 if we are to discriminate between these possibilities.

3.5. The Appearance of Bimodality in Records of CO_2, $\delta^{18}O$ and Others

We can also assess the occurrence of enhanced millennial power and climatic decoupling with respect to each of our key climate parameters. In Figure 7 we bin the records of ice rafting and millennial power from ODP Site 983 according to the range of each parameter. We also plot the temporal histograms of each parameter and their trajectories in AAT-space (lowermost plots in Figure 7a–7f), which highlight their non-linear (decoupled from AAT) pathways from IG-G state. The glacial mode of each parameter (low AAT, low CO_2, high benthic $\delta^{18}O$, high dust accumulation, low sea surface temperature) is aligned with the most intense ice rafting at Site 983, while the highest amplitude of millennial power at Site 983 coincides with a local minimum in the temporal histogram (for all parameters except AAT), sandwiched between the glacial mode and a second mode that is closer to interglacial conditions (which we name the sub-glacial mode). This local minimum gives rise to the appearance of bimodality within all histograms except that for AAT. Note that we are not concerned if the distributions are truly bimodal in a statistical sense. We use the term here to highlight the fact that each of the parameters of interest spends less time within a range aligned with a maximum in millennial power (the sweet spot) than it does on either side of that range.

As noted previously for benthic $\delta^{18}O$ and CO_2 (Barker & Knorr, 2021), the sweet spot of millennial power (blue boxes in Figure 7) appears to represent a local repeller (opposite of an attractor) where the feedback interactions between millennial and orbital variations become strongest (hence we observe local minima in the temporal histograms of CO_2 etc, which are aligned with the sweet spot in each case). We suggest that this repeller is responsible for climatic decoupling during IG-G transitions by accelerating Antarctic (and deep ocean) cooling while CO_2 (etc.) is held in a sub-glacial state before transitioning abruptly to its glacial mode (see previous discussion in Section 3.4). Accordingly, we find that the sweet spot in AAT-space (i.e., maximum millennial power with respect to AAT; Figure 7a) is aligned with a maximum in climatic decoupling (i.e., maximum offset between CO_2 etc. vs. AAT; Figure 7g). For each of the other parameters, maximum decoupling (between CO_2 and AAT in this case) is more closely aligned with the sub-glacial mode (gray subsets of each histogram). Thus the bimodality observed in records of CO_2, benthic $\delta^{18}O$ etc during the past 800 kyr appears to be a direct consequence of enhanced millennial activity and climate decoupling during the descent into full glacial conditions. The apparent lack of bimodality in the record of AAT reflects the acceleration of cooling toward its glacial mode by (we suggest) enhanced millennial activity, which simultaneously holds up the other key parameters considered here.

A second window of decoupling for some parameters is observed for more interglacial-like values of AAT (Figure 7g). This window is associated with a minor interglacial-like mode in the histograms of CO_2 and benthic $\delta^{18}O$ (Figures 7b and 7c) and appears to reflect the initial departure of AAT from full interglacial conditions over the past 400 kyr or so (i.e., since MIS 11; Figure 5). Notably this mode of decoupling is not associated with high amplitude millennial activity according to our analysis.

3.5.1. Global Expressions of Decoupling and Bimodality

Previously we discussed the transition from a sub-glacial to full glacial mode of CO_2 in terms of an increase in storage capacity by an expansion of SSW and concomitant increase in deep ocean stratification, but some further discussion of the bimodality observed (Figures 5 and 7) in records of benthic $\delta^{18}O$, dust accumulation and North Atlantic surface temperatures is warranted. The record of Antarctic dust accumulation (Figures 5 and 7d) reflects the supply, uplift and transport of dust originating in southern South America, with current evidence pointing to the strength and prevalence of strong winds ("gustiness") in the source region (McGee et al., 2010) and loss during atmospheric transport (through rainout; Markle et al., 2018) as the dominating factors in addition to variations in source availability. Increased glacial dustiness would then result from enhanced latitudinal temperature gradients and the equatorward shift and strengthening of mid latitude fronts and jets (Lambert et al., 2012; McGee et al., 2010) in combination with the shift to colder temperatures (Markle et al., 2018). The decoupling we observe between dust accumulation and AAT (Figure 7g) could then reflect the relatively late and rapid adjustment of atmospheric circulation patterns associated with the transition to full glacial conditions (Figure 5).

Sea surface temperature records from the North Atlantic are well known to reflect the abrupt shifts associated with DO variability (Bond et al., 1993; Martrat et al., 2007; N. J. Shackleton et al., 2000) and we might expect these records to exhibit a bimodal distribution, reflecting the repeated and abrupt oscillations between warm versus cold conditions. We might also expect the appearance of decoupling (with respect to AAT) whenever millennial activity is present if the time-averaged conditions are warmer as a result. Indeed the record of %NPS from ODP Site 983 is quasi-binary in nature and this is reflected by a relatively wide minimum in its temporal histogram (Figure 7f), which is (unsurprisingly) aligned with a broad maximum in millennial power. Nevertheless, we note that decoupling between 983%NPS and AAT shares the same trends with respect to obliquity and precession as CO_2, dustiness etc (Figure 6). This reflects the fact that millennial power at this site is greatest during the windows of decoupling associated with IG-G transitions (Figure 5).

The alkenone-based SST record from the Iberian Margin (Martrat et al., 2007; Rodrigues et al., 2017) also displays bimodality (with the appearance of a weak third mode representing extremely cold stadial conditions; Davtian & Bard, 2023) but the local minimum (and corresponding maximum in millennial power) is relatively much narrower than for 983%NPS and closer to interglacial conditions. Notably the DO oscillations of MIS 3 generally fall within the glacial mode at this site (Figure 5), while the fluctuations associated with IG-G transitions define the bimodality, apparently reflecting their larger and/or more abrupt nature.

3.5.2. Implications of Bimodality in Benthic $\delta^{18}O$ for Assessing Ice Sheet Expansion During Glaciation

Records of benthic $\delta^{18}O$ represent a convolution of deep ocean temperature and global ice volume. Attempts have been made to deconvolve these signals for example, by the combination of benthic foraminiferal Mg/Ca and $\delta^{18}O$ to produce a reconstruction of $\delta^{18}O_{seawater}$. Elderfield et al. (2012) produced one such reconstruction and their results suggest that, within the 100 kyr world, deep ocean temperature tends to decrease early within a glacial cycle and is followed by the build-up of continental ice sheets, a conclusion also reached by other studies (Shakun et al., 2015; Sosdian & Rosenthal, 2009). These results are reminiscent of the early cooling of AAT and MOT during the MIS 5/4 transition, and the later fall in sea level as reconstructed from coral reef terraces (Figure 1). We tentatively suggest therefore that the bimodality apparent in benthic $\delta^{18}O$ over the past 800 kyr (Figure 7) represents the decoupling of deep ocean cooling from the subsequent (and relatively more rapid) growth of continental ice sheets across IG-G transitions. A definitive test of this assertion awaits higher resolution reconstructions of ice volume and deep ocean temperature across key transitions.

3.6. A Change in IG-G Dynamics Across the MPT?

The MPT (~1.2–0.8 Ma) marked an increase in the duration and intensity of glacial cycles in the absence of any change in orbital forcing. Accordingly, the ultimate driver of change across the MPT has been the focus of many

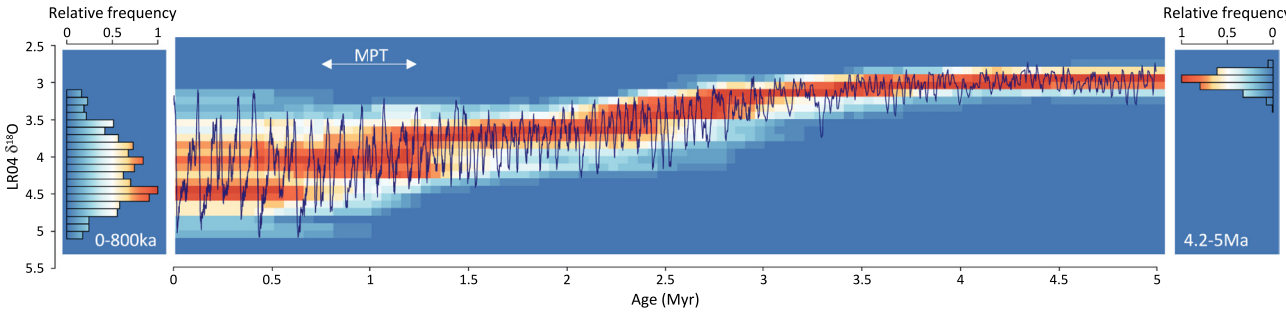

Figure 8. Emergence of bimodality across the Mid Pleistocene Transition (MPT). The LR04 benthic $\delta^{18}O$ stack (Lisiecki & Raymo, 2005) (dark blue curve) underlain by a Hovmöller diagram to show the evolution of dominant modes within the record of benthic $\delta^{18}O$ over the past 5 Myr. Each 50 kyr interval represents 800 kyr of record. Colors represent relative frequency (max = 1) as shown in the scales for the left and righthand histograms, which represent the 0–800 ka and 4.2–5 Ma intervals respectively. The local minimum centered on $\delta^{18}O = 4.25‰$ within the 0–800 ka interval is the same as that which is aligned with a maximum in millennial power at ODP Site 983 as shown in Figures 5 and 7. Bimodality is apparent following the MPT whereas the record is essentially unimodal during the Pliocene and early Pleistocene (see also Figure S10 in Supporting Information S1).

studies, with explanations ranging from a long-term decrease in atmospheric CO_2 to the removal of an erodible substrate across North America or changes in deep versus shallow circulation patterns within the Atlantic Ocean (Barker et al., 2021; Clark et al., 2006; McClymont et al., 2013; Pena & Goldstein, 2014). Beyond the growth of larger ice sheets, the MPT witnessed a pronounced shift in deep ocean water mass configuration, manifest as an increase in glacial ocean stratification with respect to nutrients and deep water endmembers (NADW vs. SSW) that may have provided the increased capacity for carbon storage during glacial periods (Farmer et al., 2019; Lear et al., 2016). We have already argued that the occurrence of high amplitude millennial variability plays an important role in the development of such conditions, giving rise to the appearance of bimodality in the records of CO_2 and benthic $\delta^{18}O$ among others. Here we question whether these processes acted in a similar manner prior to the MPT.

In Figure 8 we show how the temporal distribution of benthic $\delta^{18}O$ (Lisiecki & Raymo, 2005) has evolved since 5 Ma. This analysis suggests that bimodality in $\delta^{18}O$ has existed only since the MPT with the record being essentially unimodal before that time (see also Figure S10 in Supporting Information S1). A first order inference from this is that the dynamics associated with IG-G transitions (which we have been discussing) were somehow different prior to the emergence of extreme glacial conditions characteristic of the 100 kyr world. By extension, and because orbital forcing remained unchanged across the MPT, this implies that millennial variability associated with transitions to a glacial state prior to the MPT did not influence the relative evolution of cooling versus atmospheric CO_2 and ice volume in the same manner as in more recent times. And yet the evidence suggests that millennial variability occurred frequently before the MPT (Billups & Scheinwald, 2014; Birner et al., 2016; Hodell et al., 2023; Raymo et al., 1998).

Our results therefore provoke some key questions about the climate dynamics associated with glacial cycles prior to the MPT (i.e., within the 41 kyr world). If millennial activity coincided with IG-G transitions before 1.2 Ma, how did deep ocean and Antarctic temperatures respond? If enhanced glacial ocean stratification following the MPT reflects the amplified cooling associated with millennial activity during IG-G transitions, why was equivalent activity unable to promote similar conditions prior to that time? Our analysis suggests that answers to these questions might involve changes in the amplitude (and therefore impact) of abrupt AMOC oscillations across the MPT but changes in other high latitude processes might also be important (e.g., Yan et al., 2023). We therefore await future results (e.g., from new deep ice cores) that will allow us to quantitatively assess the relative timing and rates of change in for example, AAT, MOT, and atmospheric CO_2 during pre-MPT glacial transitions.

4. Conclusions

We have made a case for the importance and role of millennial-scale variability in the transitions from IG-G state over the past 800 kyr. Reconstructions of MOT imply an increase in the relative volume and or salinity of SSW in order to maintain a positive density contrast between SSW and NADW during recent glacial periods MIS 2 and 4. Our calculations suggest that such water mass reconfiguration became inevitable during the MIS 5/4 transition

due in part to the enhanced cooling associated with extreme climate oscillations at that time. More specifically we suggest that extreme oscillations of the AMOC, in combination with cooler northern hemisphere summers primarily as a function of low obliquity, act to promote deep ocean cooling and increase the relative volume and or salinity of SSW during IG-G transitions in general, thereby providing the additional storage capacity necessary for enhanced glacial storage of atmospheric CO_2.

During such transitions, we observe decoupling between AAT and other key climate parameters including CO_2 and benthic $\delta^{18}O$, reflecting the delayed and subsequently abrupt transition to full glacial conditions and giving rise to the appearance of bimodality within these timeseries. We use this observation, and the lack of apparent bimodality in the timeseries of benthic $\delta^{18}O$ prior to the MPT, to suggest that a change in the dynamics of IG-G transitions must have occurred across the MPT. We must now wait for new reconstructions of ocean circulation, Antarctic and deep ocean temperature, atmospheric CO_2 content and ice volume that will allow us to improve our understanding of glacial transitions before and after the MPT.

Data Availability Statement

Data on which this article is based can be found in Barker et al. (2019), Bereiter et al. (2015, 2018), Berger and Loutre (1991), Cheng et al. (2016), Davtian and Bard (2023), Lambert et al. (2012), Lisiecki and Raymo (2005), Martrat et al. (2007), Mayewski et al. (1997), Nehrbass-Ahles et al. (2020), NGRIP_members (2004), Parrenin et al. (2013), Rodrigues et al. (2017), N. J. Shackleton et al. (2000), and S. Shackleton et al. (2020, 2021).

Acknowledgments
We thank the authors of all datasets used here for making their results freely available. This study contributes to the Helmholtz research programme "Changing Earth—Sustaining our Future" and the German Paleomodelling Research Project PalMod, funded by the BMBF. We thank P. C. Tzedakis for advice on MIS nomenclature. We thank three anonymous reviewers for their constructive suggestions. This is Cardiff EARTH CRediT contribution #10. Open Access funding enabled and organized by Projekt DEAL.

References

Adkins, J. F. (2013). The role of deep ocean circulation in setting glacial climates. *Paleoceanography*, *28*(3), 539–561. https://doi.org/10.1002/palo.20046

Adkins, J. F., McIntyre, K., & Schrag, D. P. (2002). The salinity, temperature, and $\delta^{18}O$ of the glacial deep ocean. *Science*, *298*(5599), 1769–1773. https://doi.org/10.1126/science.1076252

Ahn, J., & Brook, E. J. (2008). Atmospheric CO_2 and climate on millennial time scales during the last glacial period. *Science*, *322*(5898), 83–85. https://doi.org/10.1126/science.1160832

Barker, S. (2005). The 'flickering switch' of late Pleistocene climate change revisited. *Geophysical Research Letters*, *32*(24), 24703. https://doi.org/10.1029/2005gl024486

Barker, S., Chen, J., Gong, X., Jonkers, L., Knorr, G., & Thornalley, D. (2015). Icebergs not the trigger for North Atlantic cold events. *Nature*, *520*(7547), 333–336. https://doi.org/10.1038/nature14330

Barker, S., & Diz, P. (2014). Timing of the descent into the last ice age determined by the bipolar seesaw. *Paleoceanography*, *29*(6), 489–507. https://doi.org/10.1002/2014pa002623

Barker, S., & Knorr, G. (2007). Antarctic climate signature in the Greenland ice core record. *Proceedings of the National Academy of Sciences of the United States of America*, *104*(44), 17278–17282. https://doi.org/10.1073/pnas.0708494104

Barker, S., & Knorr, G. (2021). Millennial scale feedbacks determine the shape and rapidity of glacial termination. *Nature Communications*, *12*(1), 2273. https://doi.org/10.1038/s41467-021-22388-6

Barker, S., Knorr, G., Conn, S., Lordsmith, S., Newman, D., & Thornalley, D. (2019). Early interglacial legacy of deglacial climate instability. *Paleoceanography and Paleoclimatology*, *34*(8), 1455–1475. https://doi.org/10.1029/2019PA003661

Barker, S., Knorr, G., Edwards, R. L., Parrenin, F., Putnam, A. E., Skinner, L. C., et al. (2011). 800,000 years of abrupt climate variability. *Science*, *334*(6054), 347–351. https://doi.org/10.1126/science.1203580

Barker, S., Knorr, G., Vautravers, M., Diz, P., & Skinner, L. C. (2010). Extreme deepening of the Atlantic overturning circulation during deglaciation. *Nature Geoscience*, *3*(8), 567–571. https://doi.org/10.1038/NGEO1921

Barker, S., Zhang, X., Jonkers, L., Lordsmith, S., Conn, S., & Knorr, G. (2021). Strengthening Atlantic inflow across the mid-Pleistocene transition. *Paleoceanography and Paleoclimatology*, *36*(4), e2020PA004200. https://doi.org/10.1029/2020PA004200

Barnola, J. M., Raynaud, D., Korotkevich, Y. S., & Lorius, C. (1987). Vostok ice core provides 160,000-year record of atmospheric CO_2. *Nature*, *329*(6138), 408–414. https://doi.org/10.1038/329408a0

Baumgarter, A., & Reichel, E. (1975). *The world water balance* (Vol. 179). Elsevier.

Bazin, L., Landais, A., Lemieux-Dudon, B., Toyé Mahamadou Kele, H., Veres, D., Parrenin, F., et al. (2013). An optimized multi-proxy, multi-site Antarctic ice and gas orbital chronology (AICC2012): 120–800 ka. *Climate of the Past*, *9*(4), 1715–1731. https://doi.org/10.5194/cp-9-1715-2013

Bereiter, B., Eggleston, S., Schmitt, J., Nehrbass-Ahles, C., Stocker, T. F., Fischer, H., et al. (2015). Revision of the EPICA Dome C CO_2 record from 800 to 600 kyr before present. *Geophysical Research Letters*, *42*(2), 542–549. https://doi.org/10.1002/2014gl061957

Bereiter, B., Luthi, D., Siegrist, M., Schupbach, S., Stocker, T. F., & Fischer, H. (2012). Mode change of millennial CO_2 variability during the last glacial cycle associated with a bipolar marine carbon seesaw. *Proceedings of the National Academy of Sciences of the United States of America*, *109*(25), 9755–9760. https://doi.org/10.1073/pnas.1204069109

Bereiter, B., Shackleton, S., Baggenstos, D., Kawamura, K., & Severinghaus, J. (2018). Mean global ocean temperatures during the last glacial transition. *Nature*, *553*(7686), 39–44. https://doi.org/10.1038/nature25152

Berger, A., & Loutre, M. F. (1991). Insolation values for the climate of the last 10 million years. *Quaternary Science Reviews*, *10*(4), 297–317. https://doi.org/10.1016/0277-3791(91)90033-q

Billups, K., & Scheinwald, A. (2014). Origin of millennial-scale climate signals in the subtropical North Atlantic. *Paleoceanography*, *29*(6), 612–627. https://doi.org/10.1002/2014pa002641

Bintanja, R., van de Wal, R. S., & Oerlemans, J. (2005). Modelled atmospheric temperatures and global sea levels over the past million years. *Nature*, *437*(7055), 125–128. https://doi.org/10.1038/nature03975

Birner, B., Hodell, D., Tzedakis, P., & Skinner, L. (2016). Similar millennial climate variability on the Iberian margin during two early Pleistocene glacials and MIS 3. *Paleoceanography*, *31*(1), 203–217. https://doi.org/10.1002/2015pa002868

Biscaye, P. E., Grousset, F. E., Revel, M., VanderGaast, S., Zielinski, G. A., Vaars, A., & Kukla, G. (1997). Asian provenance of glacial dust (stage 2) in the Greenland ice sheet project 2 ice core, Summit, Greenland. *Journal of Geophysical Research*, *102*(C12), 26765–26781. https://doi.org/10.1029/97jc01249

Blunier, T., & Brook, E. J. (2001). Timing of millennial-scale climate change in Antarctica and Greenland during the last glacial period. *Science*, *291*(5501), 109–112. https://doi.org/10.1126/science.291.5501.109

Böhm, E., Lippold, J., Gutjahr, M., Frank, M., Blaser, P., Antz, B., et al. (2015). Strong and deep Atlantic meridional overturning circulation during the last glacial cycle. *Nature*, *517*(7532), 73–76. https://doi.org/10.1038/nature14059

Bond, G., Broecker, W., Johnsen, S., McManus, J., Labeyrie, L., Jouzel, J., & Bonani, G. (1993). Correlations between climate records from North-Atlantic sediments and Greenland ice. *Nature*, *365*(6442), 143–147. https://doi.org/10.1038/365143a0

Broecker, W. S., & Denton, G. H. (1989). The role of ocean-atmosphere reorganizations in glacial cycles. *Geochimica et Cosmochimica Acta*, *53*(10), 2465–2501. https://doi.org/10.1016/0016-7037(89)90123-3

Browaeys, J. (2023). Linear fit with both uncertainties in x and in y. In *MATLAB central file exchange*. Retrieved from https://www.mathworks.com/matlabcentral/fileexchange/45711-linear-fit-with-both-uncertainties-in-x-and-in-y

Buizert, C., Fudge, T., Roberts, W. H., Steig, E. J., Sherriff-Tadano, S., Ritz, C., et al. (2021). Antarctic surface temperature and elevation during the last glacial maximum. *Science*, *372*(6546), 1097–1101. https://doi.org/10.1126/science.abd2897

Chappell, J., & Shackleton, N. J. (1986). Oxygen isotopes and sea-level. *Nature*, *324*(6093), 137–140. https://doi.org/10.1038/324137a0

Cheng, H., Edwards, R. L., Broecker, W. S., Denton, G. H., Kong, X. G., Wang, Y. J., et al. (2009). Ice age terminations. *Science*, *326*(5950), 248–252. https://doi.org/10.1126/science.1177840

Cheng, H., Edwards, R. L., Sinha, A., Spötl, C., Yi, L., Chen, S., et al. (2016). The Asian monsoon over the past 640,000 years and ice age terminations. *Nature*, *534*(7609), 640–646. https://doi.org/10.1038/nature18591

Clark, P. U., Archer, D., Pollard, D., Blum, J. D., Rial, J. A., Brovkin, V., et al. (2006). The middle Pleistocene transition: Characteristics. Mechanisms, and implications for long-term changes in atmospheric PCO2. *Quaternary Science Reviews*, *25*(23–24), 3150–3184. https://doi.org/10.1016/j.quascirev.2006.07.008

Crowley, T. J. (1992). North Atlantic deep water cools the southern hemisphere. *Paleoceanography*, *7*(4), 489–497. https://doi.org/10.1029/92pa01058

Curry, W. B. (1996). Late Quaternary deep circulation in the western equatorial Atlantic. In G. Wefer, W. H. Berger, G. Siedler, & D. J. Webb (Eds.), *The South Atlantic: Present and past circulation* (pp. 577–598). Springer-Verlag.

Curry, W. B., & Oppo, D. W. (2005). Glacial water mass geometry and the distribution of $\delta^{13}C$ of ΣCO_2 in the western Atlantic Ocean. *Paleoceanography*, *20*(1). https://doi.org/10.1029/2004PA001021

Cutler, K. B., Edwards, R. L., Taylor, F. W., Cheng, H., Adkins, J., Gallup, C. D., et al. (2003). Rapid sea-level fall and deep-ocean temperature change since the last interglacial period. *Earth and Planetary Science Letters*, *206*(3–4), 253–271. https://doi.org/10.1016/s0012-821x(02)01107-x

Davtian, N., & Bard, E. (2023). A new view on abrupt climate changes and the bipolar seesaw based on paleotemperatures from Iberian Margin sediments. *Proceedings of the National Academy of Sciences*, *120*(12), e2209558120. https://doi.org/10.1073/pnas.2209558120

Denton, G. H., Anderson, R. F., Toggweiler, J. R., Edwards, R. L., Schaefer, J. M., & Putnam, A. E. (2010). The last glacial termination. *Science*, *328*(5986), 1652–1656. https://doi.org/10.1126/science.1184119

Doughty, A. M., Kaplan, M. R., Peltier, C., & Barker, S. (2021). A maximum in global glacier extent during MIS 4. *Quaternary Science Reviews*, *261*, 106948. https://doi.org/10.1016/j.quascirev.2021.106948

Elderfield, H., Ferretti, P., Greaves, M., Crowhurst, S., McCave, I. N., Hodell, D., & Piotrowski, A. M. (2012). Evolution of ocean temperature and ice volume through the mid-Pleistocene climate transition. *Science*, *337*(6095), 704–709. https://doi.org/10.1126/science.1221294

Farmer, J., Hönisch, B., Haynes, L., Kroon, D., Jung, S., Ford, H., et al. (2019). Deep Atlantic Ocean carbon storage and the rise of 100,000-year glacial cycles. *Nature Geoscience*, *12*(5), 355–360. https://doi.org/10.1038/s41561-019-0334-6

Ferrari, R., Jansen, M. F., Adkins, J. F., Burke, A., Stewart, A. L., & Thompson, A. F. (2014). Antarctic sea ice control on ocean circulation in present and glacial climates. *Proceedings of the National Academy of Sciences*, *111*(24), 8753–8758. https://doi.org/10.1073/pnas.1323922111

Fuhrer, K., Wolff, E. W., & Johnsen, S. J. (1999). Timescales for dust variability in the Greenland Ice Core Project (GRIP) ice core in the last 100,000 years. *Journal of Geophysical Research*, *104*(D24), 31043–31052.

Galbraith, E. D., & de Lavergne, C. (2019). Response of a comprehensive climate model to a broad range of external forcings: Relevance for deep ocean ventilation and the development of late Cenozoic ice ages. *Climate Dynamics*, *52*(1–2), 653–679. https://doi.org/10.1007/s00382-018-4157-8

Galbraith, E. D., Merlis, T. M., & Palter, J. B. (2016). Destabilization of glacial climate by the radiative impact of Atlantic Meridional Overturning Circulation disruptions. *Geophysical Research Letters*, *43*(15), 8214–8221. https://doi.org/10.1002/2016gl069846

Gill, A. (1983). *Atmosphere-Ocean dynamics*. Academic Press.

Hasenclever, J., Knorr, G., Rüpke, L. H., Köhler, P., Morgan, J., Garofalo, K., et al. (2017). Sea level fall during glaciation stabilized atmospheric CO_2 by enhanced volcanic degassing. *Nature Communications*, *8*(1), 15867. https://doi.org/10.1038/ncomms15867

Henry, L., McManus, J. F., Curry, W. B., Roberts, N. L., Piotrowski, A. M., & Keigwin, L. D. (2016). North Atlantic Ocean circulation and abrupt climate change during the last glaciation. *Science*, *353*(6298), 470–474. https://doi.org/10.1126/science.aaf5529

Hines, S. K., Bolge, L., Goldstein, S. L., Charles, C. D., Hall, I. R., & Hemming, S. R. (2021). Little change in ice age water mass structure from Cape Basin benthic neodymium and carbon isotopes. *Paleoceanography and Paleoclimatology*, *36*(11), e2021PA004281. https://doi.org/10.1029/2021pa004281

Hodell, D. A., Crowhurst, S. J., Lourens, L., Margari, V., Nicolson, J., Rolfe, J. E., et al. (2023). A 1.5-million-year record of orbital and millennial climate variability in the North Atlantic. *Climate of the Past*, *19*(3), 607–636. https://doi.org/10.5194/cp-19-607-2023

Imbrie, J., Berger, A., Boyle, E. A., Clemens, S. C., Duffy, A., Howard, W. R., et al. (1993). On the structure and origin of major glaciation cycles 2. The 100,000-year cycle. *Paleoceanography*, *8*(6), 699–735. https://doi.org/10.1029/93pa02751

Insua, T. L., Spivack, A. J., Graham, D., D'Hondt, S., & Moran, K. (2014). Reconstruction of Pacific ocean bottom water salinity during the last glacial maximum. *Geophysical Research Letters*, *41*(8), 2914–2920. https://doi.org/10.1002/2014gl059575

Johnson, G. C. (2008). Quantifying Antarctic bottom water and North Atlantic deep water volumes. *Journal of Geophysical Research*, *113*(C5), C05027. https://doi.org/10.1029/2007jc004477

Jouzel, J., Masson-Delmotte, V., Cattani, O., Dreyfus, G., Falourd, S., Hoffmann, G., et al. (2007). Orbital and millennial Antarctic climate variability over the past 800,000 years. *Science*, *317*(5839), 793–796. https://doi.org/10.1126/science.1141038

Kawamura, K., Abe-Ouchi, A., Motoyama, H., Ageta, Y., Aoki, S., Azuma, N., et al. (2017). State dependence of climatic instability over the past 720,000 years from Antarctic ice cores and climate modeling. *Science Advances*, *3*(2), e1600446. https://doi.org/10.1126/sciadv.1600446

Keigwin, L. D., Curry, W. B., Lehman, S. J., & Johnsen, S. (1994). The role of the deep-ocean in North-Atlantic climate-change between 70-kyr and 130-kyr ago. *Nature*, *371*(6495), 323–326. https://doi.org/10.1038/371323a0

Keigwin, L. D., & Swift, S. A. (2017). Carbon isotope evidence for a northern source of deep water in the glacial western North Atlantic. *Proceedings of the National Academy of Sciences*, *114*(11), 2831–2835. https://doi.org/10.1073/pnas.1614693114

Kindler, P., Guillevic, M., Baumgartner, M. F., Schwander, J., Landais, A., & Leuenberger, M. (2014). Temperature reconstruction from 10 to 120 kyr b2k from the NGRIP ice core. *Climate of the Past*, *10*(2), 887–902. https://doi.org/10.5194/cp-10-887-2014

Kirst, G. J., Schneider, R. R., Muller, P. J., von Storch, I., & Wefer, G. (1999). Late Quaternary temperature variability in the Benguela current system derived from alkenones. *Quaternary Research*, *52*(1), 92–103. https://doi.org/10.1006/qres.1999.2040

Kissel, C., Laj, C., Piotrowski, A. M., Goldstein, S. L., & Hemming, S. R. (2008). Millennial-scale propagation of Atlantic deep waters to the glacial Southern Ocean. *Paleoceanography*, *23*(2), PA2102. https://doi.org/10.1029/2008PA001624

Knorr, G., Barker, S., Zhang, X., Lohmann, G., Gong, X., Gierz, P., et al. (2021). A salty deep ocean as a prerequisite for glacial termination. *Nature Geoscience*, *14*(12), 930–936. https://doi.org/10.1038/s41561-021-00857-3

Köhler, P., Knorr, G., Stap, L. B., Ganopolski, A., de Boer, B., van de Wal, R. S., et al. (2018). The effect of obliquity-driven changes on paleoclimate sensitivity during the late Pleistocene. *Geophysical Research Letters*, *45*(13), 6661–6671. https://doi.org/10.1029/2018gl077717

Köhler, P., & Munhoven, G. (2020). Late Pleistocene carbon cycle revisited by considering solid Earth processes. *Paleoceanography and Paleoclimatology*, *35*(12), e2020PA004020. https://doi.org/10.1029/2020pa004020

Lambert, F., Bigler, M., Steffensen, J. P., Hutterli, M., & Fischer, H. (2012). Centennial mineral dust variability in high-resolution ice core data from Dome C, Antarctica. *Climate of the Past*, *8*(2), 609–623. https://doi.org/10.5194/cp-8-609-2012

Lear, C. H., Billups, K., Rickaby, R. E., Diester-Haass, L., Mawbey, E. M., & Sosdian, S. M. (2016). Breathing more deeply: Deep ocean carbon storage during the mid-Pleistocene climate transition. *Geology*, *44*(12), 1035–1038. https://doi.org/10.1130/g38636.1

Legrand, M., Hammer, C., DeAngelis, M., Savarino, J., Delmas, R., Clausen, H., & Johnsen, S. J. (1997). Sulfur-containing species (methanesulfonate and SO_4) over the last climatic cycle in the Greenland Ice Core Project (central Greenland) ice core. *Journal of Geophysical Research*, *102*(C12), 26663–26679. https://doi.org/10.1029/97jc01436

Li, C., Battisti, D. S., Schrag, D. P., & Tziperman, E. (2005). Abrupt climate shifts in Greenland due to displacements of the sea ice edge. *Geophysical Research Letters*, *32*(19), L19702. https://doi.org/10.1029/2005gl023492

Lisiecki, L. E., & Raymo, M. E. (2005). A Pliocene-Pleistocene stack of 57 globally distributed benthic $\delta^{18}O$ records. *Paleoceanography*, *20*(2), PA1003. https://doi.org/10.1029/2004PA001071

Lynch-Stieglitz, J., Adkins, J. F., Curry, W. B., Dokken, T., Hall, I. R., Herguera, J. C., et al. (2007). Atlantic meridional overturning circulation during the last glacial maximum. *Science*, *316*(5821), 66–69. https://doi.org/10.1126/science.1137127

Lynch-Stieglitz, J., Schmidt, M. W., Gene Henry, L., Curry, W. B., Skinner, L. C., Mulitza, S., et al. (2014). Muted change in Atlantic overturning circulation over some glacial-aged Heinrich events. *Nature Geoscience*, *7*(2), 144–150. https://doi.org/10.1038/ngeo2045

Marcott, S. A., Bauska, T. K., Buizert, C., Steig, E. J., Rosen, J. L., Cuffey, K. M., et al. (2014). Centennial-scale changes in the global carbon cycle during the last deglaciation. *Nature*, *514*(7524), 616–619. https://doi.org/10.1038/nature13799

Markle, B. R., Steig, E. J., Roe, G. H., Winckler, G., & McConnell, J. R. (2018). Concomitant variability in high-latitude aerosols, water isotopes and the hydrologic cycle. *Nature Geoscience*, *11*(11), 853–859. https://doi.org/10.1038/s41561-018-0210-9

Martin, K. C., Buizert, C., Edwards, J. S., Kalk, M. L., Riddell-Young, B., Brook, E. J., et al. (2023). Bipolar impact and phasing of Heinrich-type climate variability. *Nature*, *617*(7959), 1–5. https://doi.org/10.1038/s41586-023-05875-2

Martrat, B., Grimalt, J. O., Shackleton, N. J., de Abreu, L., Hutterli, M. A., & Stocker, T. F. (2007). Four climate cycles of recurring deep and surface water destabilizations on the Iberian margin. *Science*, *317*(5837), 502–507. https://doi.org/10.1126/science.1139994

Mayewski, P. A., Meeker, L. D., Twickler, M. S., Whitlow, S., Yang, Q. Z., Lyons, W. B., & Prentice, M. (1997). Major features and forcing of high-latitude northern hemisphere atmospheric circulation using a 110,000-year-long glaciochemical series. *Journal of Geophysical Research*, *102*(C12), 26345–26366. https://doi.org/10.1029/96jc03365

McClymont, E. L., Sosdian, S. M., Rosell-Melé, A., & Rosenthal, Y. (2013). Pleistocene sea-surface temperature evolution: Early cooling, delayed glacial intensification, and implications for the mid-Pleistocene climate transition. *Earth-Science Reviews*, *123*, 173–193. https://doi.org/10.1016/j.earscirev.2013.04.006

McDougall, T. J. (1987). Thermobaricity, cabbeling, and water-mass conversion. *Journal of Geophysical Research*, *92*(C5), 5448–5464.

McGee, D., Broecker, W. S., & Winckler, G. (2010). Gustiness: The driver of glacial dustiness? *Quaternary Science Reviews*, *29*(17–18), 2340–2350. https://doi.org/10.1016/j.quascirev.2010.06.009

McManus, J. F., Francois, R., Gherardi, J. M., Keigwin, L. D., & Brown-Leger, S. (2004). Collapse and rapid resumption of Atlantic meridional circulation linked to deglacial climate changes. *Nature*, *428*(6985), 834–837. https://doi.org/10.1038/nature02494

McManus, J. F., Oppo, D. W., & Cullen, J. L. (1999). A 0.5-million-year record of millennial-scale climate variability in the North Atlantic. *Science*, *283*(5404), 971–975. https://doi.org/10.1126/science.283.5404.971

Menking, J. A., Shackleton, S. A., Bauska, T. K., Buffen, A. M., Brook, E. J., Barker, S., et al. (2022). Multiple carbon cycle mechanisms associated with the glaciation of Marine Isotope Stage 4. *Nature Communications*, *13*(1), 1–10. https://doi.org/10.1038/s41467-022-33166-3

Miller, M., Adkins, J., Menemenlis, D., & Schodlok, M. (2012). The role of ocean cooling in setting glacial southern source bottom water salinity. *Paleoceanography*, *27*(3), PA3207. https://doi.org/10.1029/2012PA002297

Nehrbass-Ahles, C., Shin, J., Schmitt, J., Bereiter, B., Joos, F., Schilt, A., et al. (2020). Abrupt CO_2 release to the atmosphere under glacial and early interglacial climate conditions. *Science*, *369*(6506), 1000–1005. https://doi.org/10.1126/science.aay8178

NGRIP_members. (2004). High-resolution record of Northern Hemisphere climate extending into the last interglacial period. *Nature*, *431*(7005), 147–151. https://doi.org/10.1038/nature02805

Oppo, D. W., Gebbie, G., Huang, K. F., Curry, W. B., Marchitto, T. M., & Pietro, K. R. (2018). Data constraints on glacial Atlantic water mass geometry and properties. *Paleoceanography and Paleoclimatology*, *33*(9), 1013–1034. https://doi.org/10.1029/2018pa003408

Otto-Bliesner, B., Hewitt, C., Marchitto, T., Brady, E., Abe-Ouchi, A., Crucifix, M., et al. (2007). Last glacial maximum ocean thermohaline circulation: PMIP2 model intercomparisons and data constraints. *Geophysical Research Letters*, *34*(12), L12706. https://doi.org/10.1029/2007gl029475

Parrenin, F., Barker, S., Blunier, T., Chappellaz, J., Jouzel, J., Landais, A., et al. (2012). On the gas-ice depth difference (Δdepth) along the EPICA Dome C ice core. *Climate of the Past*, *8*(4), 1239–1255. https://doi.org/10.5194/cp-8-1239-2012

Parrenin, F., Masson-Delmotte, V., Kohler, P., Raynaud, D., Paillard, D., Schwander, J., et al. (2013). Synchronous change of atmospheric CO_2 and Antarctic temperature during the last deglacial warming. *Science*, *339*(6123), 1060–1063. https://doi.org/10.1126/science.1226368

Pausata, F. S. R., Battisti, D. S., Nisancioglu, K. H., & Bitz, C. M. (2011). Chinese stalagmite delta O-18 controlled by changes in the Indian monsoon during a simulated Heinrich event. *Nature Geoscience*, *4*(7), 474–480. https://doi.org/10.1038/ngeo1169

Pedro, J. B., Andersson, C., Vettoretti, G., Voelker, A., Waelbroeck, C., Dokken, T. M., et al. (2022). Dansgaard-Oeschger and Heinrich event temperature anomalies in the North Atlantic set by sea ice, frontal position and thermocline structure. *Quaternary Science Reviews*, *289*, 107599. https://doi.org/10.1016/j.quascirev.2022.107599

Pedro, J. B., Jochum, M., Buizert, C., He, F., Barker, S., & Rasmussen, S. O. (2018). Beyond the bipolar seesaw: Toward a process understanding of interhemispheric coupling. *Quaternary Science Reviews*, *192*, 27–46. https://doi.org/10.1016/j.quascirev.2018.05.005

Pena, L. D., & Goldstein, S. L. (2014). Thermohaline circulation crisis and impacts during the mid-Pleistocene transition. *Science*, *345*(6194), 318–322. https://doi.org/10.1126/science.1249770

Piotrowski, A. M., Goldstein, S. L., Hemming, S. R., & Fairbanks, R. G. (2005). Temporal relationships of carbon cycling and ocean circulation at glacial boundaries. *Science*, *307*(5717), 1933–1938. https://doi.org/10.1126/science.1104883

Piotrowski, A. M., Goldstein, S. L., Hemming, S. R., Fairbanks, R. G., & Zylberberg, D. R. (2008). Oscillating glacial northern and southern deep water formation from combined neodymium and carbon isotopes. *Earth and Planetary Science Letters*, *272*(1–2), 394–405. https://doi.org/10.1016/j.epsl.2008.05.011

Pöppelmeier, F., Baggenstos, D., Grimmer, M., Liu, Z., Schmitt, J., Fischer, H., & Stocker, T. F. (2023). The effect of past saturation changes on noble gas reconstructions of mean ocean temperature. *Geophysical Research Letters*, *50*(6), e2022GL102055. https://doi.org/10.1029/2022gl102055

Pöppelmeier, F., Gutjahr, M., Blaser, P., Schulz, H., Süfke, F., & Lippold, J. (2021). Stable Atlantic deep water mass sourcing on glacial-interglacial timescales. *Geophysical Research Letters*, *48*(15), e2021GL092722. https://doi.org/10.1029/2021gl092722

Rasmussen, S. O., Bigler, M., Blockley, S. P., Blunier, T., Buchardt, S. L., Clausen, H. B., et al. (2014). A stratigraphic framework for abrupt climatic changes during the last glacial period based on three synchronized Greenland ice-core records: Refining and extending the INTIMATE event stratigraphy. *Quaternary Science Reviews*, *106*, 14–28. https://doi.org/10.1016/j.quascirev.2014.09.007

Raymo, M. E., Ganley, K., Carter, S., Oppo, D. W., & McManus, J. (1998). Millennial-scale climate instability during the early Pleistocene epoch. *Nature*, *392*(6677), 699–702. https://doi.org/10.1038/33658

Rodrigues, T., Alonso-García, M., Hodell, D., Rufino, M., Naughton, F., Grimalt, J., et al. (2017). A 1-Ma record of sea surface temperature and extreme cooling events in the North Atlantic: A perspective from the Iberian margin. *Quaternary Science Reviews*, *172*, 118–130. https://doi.org/10.1016/j.quascirev.2017.07.004

Ruiz-Martinez, G. (2023). Seawater density from salinity, temperature and pressure. In *MATLAB central file exchange*. Retrieved from https://www.mathworks.com/matlabcentral/fileexchange/85900-seawater-density-from-salinity-temperature-and-pressure

Schaefer, J. M., Putnam, A. E., Denton, G. H., Kaplan, M. R., Birkel, S., Doughty, A. M., et al. (2015). The southern glacial maximum 65,000 years ago and its unfinished termination. *Quaternary Science Reviews*, *114*, 52–60. https://doi.org/10.1016/j.quascirev.2015.02.009

Schulz, M. (2002). The tempo of climate change during Dansgaard-Oeschger interstadials and its potential to affect the manifestation of the 1470-year climate cycle. *Geophysical Research Letters*, *29*(1), 1002. https://doi.org/10.1029/2001gl013277

Shackleton, N. J., Hall, M. A., & Vincent, E. (2000). Phase relationships between millennial-scale events 64,000–24,000 years ago. *Paleoceanography*, *15*(6), 565–569. https://doi.org/10.1029/2000pa000513

Shackleton, S., Baggenstos, D., Menking, J., Dyonisius, M., Bereiter, B., Bauska, T., et al. (2020). Global ocean heat content in the Last Interglacial. *Nature Geoscience*, *13*(1), 77–81. https://doi.org/10.1038/s41561-019-0498-0

Shackleton, S., Menking, J. A., Brook, E., Buizert, C., Dyonisius, M. N., Petrenko, V. V., et al. (2021). Evolution of mean ocean temperature in marine isotope stage 4. *Climate of the Past*, *17*(5), 2273–2289. https://doi.org/10.5194/cp-17-2273-2021

Shakun, J. D., Lea, D. W., Lisiecki, L. E., & Raymo, M. E. (2015). An 800-kyr record of global surface ocean $\delta^{18}O$ and implications for ice volume-temperature coupling. *Earth and Planetary Science Letters*, *426*, 58–68. https://doi.org/10.1016/j.epsl.2015.05.042

Shin, S. I., Liu, Z. G., Otto-Bliesner, B. L., Kutzbach, J. E., & Vavrus, S. J. (2003). Southern Ocean sea-ice control of the glacial North Atlantic thermohaline circulation. *Geophysical Research Letters*, *30*(2), 1096. https://doi.org/10.1029/2002gl015513

Sima, A., Paul, A., & Schulz, M. (2004). The Younger Dryas—An intrinsic feature of late Pleistocene climate change at millennial timescales. *Earth and Planetary Science Letters*, *222*(3–4), 741–750. https://doi.org/10.1016/j.epsl.2004.03.026

Skinner, L. C., Shackleton, N. J., & Elderfield, H. (2003). Millennial scale variability of deep water temperature and $\delta^{18}O_{dw}$ indicating deep water source variations in the northeast Atlantic, 0–34 cal. ka BP. *Geochemistry, Geophysics, Geosystems*, *4*(12), 1098. https://doi.org/10.1029/2003GC000585

Sosdian, S., & Rosenthal, Y. (2009). Deep-sea temperature and ice volume changes across the Pliocene-Pleistocene climate transitions. *Science*, *325*(5938), 306–310. https://doi.org/10.1126/science.1169938

Stocker, T. F., & Johnsen, S. J. (2003). A minimum thermodynamic model for the bipolar seesaw. *Paleoceanography*, *18*(4), 1087. https://doi.org/10.1029/2003PA000920

Thompson, W. G., & Goldstein, S. L. (2006). A radiometric calibration of the SPECMAP timescale. *Quaternary Science Reviews*, *25*(23–24), 3207–3215. https://doi.org/10.1016/j.quascirev.2006.02.007

Thornalley, D. J. R., Barker, S., Becker, J., Knorr, G., & Hall, I. R. (2013). Abrupt changes in deep Atlantic circulation during the transition to full glacial conditions. *Paleoceanography*, *28*(2), 253–262. https://doi.org/10.1002/palo.20025

Veres, D., Bazin, L., Landais, A., ToyÃ© Mahamadou Kele, H., Lemieux-Dudon, B., Parrenin, F., et al. (2012). The Antarctic ice core chronology (AICC2012): An optimized multi-parameter and multi-site dating approach for the last 120 thousand years. *Climate of the Past Discussions*, *8*(6), 6011–6049.

Wang, Y. J., Cheng, H., Edwards, R. L., An, Z. S., Wu, J. Y., Shen, C. C., & Dorale, J. A. (2001). A high-resolution absolute-dated Late Pleistocene monsoon record from Hulu Cave, China. *Science*, *294*(5550), 2345–2348. https://doi.org/10.1126/science.1064618

Weyl, P. K. (1968). The role of the oceans in climatic change: A theory of the ice ages. *Meteorological Monographs*, *8*(30), 37–62.

Woillard, G. (1979). Abrupt end of the last interglacial s.s. in North-East France. *Nature*, *281*(5732), 558–562. https://doi.org/10.1038/281558a0

Wolff, E. W., Fischer, H., & Rothlisberger, R. (2009). Glacial terminations as southern warmings without northern control. *Nature Geoscience*, *2*(3), 206–209. https://doi.org/10.1038/ngeo442

Yan, Y., Kurbatov, A. V., Mayewski, P. A., Shackleton, S., & Higgins, J. A. (2023). Early Pleistocene East Antarctic temperature in phase with local insolation. *Nature Geoscience*, *16*(1), 50–55. https://doi.org/10.1038/s41561-022-01095-x

Yu, J., Menviel, L., Jin, Z., Thornalley, D., Barker, S., Marino, G., et al. (2016). Sequestration of carbon in the deep Atlantic during the last glaciation. *Nature Geoscience*, *9*(4), 319–324. https://doi.org/10.1038/NGEO2657

Zaucker, F., & Broecker, W. S. (1992). The influence of atmospheric moisture transport on the fresh- water balance of the Atlantic drainage-basin—General-circulation model simulations and observations. *Journal of Geophysical Research*, *97*(D3), 2765–2773. https://doi.org/10.1029/91jd01699

Zhang, X., Barker, S., Knorr, G., Lohmann, G., Drysdale, R., Sun, Y., et al. (2021). Direct astronomical influence on abrupt climate variability. *Nature Geoscience*, *14*(11), 819–826. https://doi.org/10.1038/s41561-021-00846-6

Zhang, X., Knorr, G., Lohmann, G., & Barker, S. (2017). Abrupt North Atlantic circulation changes in response to gradual CO_2 forcing in a glacial climate state. *Nature Geoscience*, *10*(7), 518–523. https://doi.org/10.1038/ngeo2974

Zhang, X., Lohmann, G., Knorr, G., & Purcell, C. (2014). Abrupt glacial climate shifts controlled by ice sheet changes. *Nature*, *512*(7514), 290–294. https://doi.org/10.1038/nature13592

Zhang, X., Lohmann, G., Knorr, G., & Xu, X. (2013). Different ocean states and transient characteristics in Last Glacial Maximum simulations and implications for deglaciation. *Climate of the Past*, *9*(5), 2319–2333. https://doi.org/10.5194/cp-9-2319-2013

References From the Supporting Information

EPICA. (2006). One-to-one coupling of glacial climate variability in Greenland and Antarctica. *Nature*, *444*(7116), 195–198. https://doi.org/10.1038/nature05301

Hodell, D., Lourens, L., Crowhurst, S., Konijnendijk, T., Tjallingii, R., Jiménez-Espejo, F., et al. (2015). A reference time scale for site U1385 (Shackleton site) on the SW Iberian margin. *Global and Planetary Change*, *133*, 49–64. https://doi.org/10.1016/j.gloplacha.2015.07.002

Marchitto, T., Curry, W., Lynch-Stieglitz, J., Bryan, S., Cobb, K., & Lund, D. (2014). Improved oxygen isotope temperature calibrations for cosmopolitan benthic foraminifera. *Geochimica et Cosmochimica Acta*, *130*, 1–11. https://doi.org/10.1016/j.gca.2013.12.034

Svensson, A., Bigler, M., Blunier, T., Clausen, H., Dahl-Jensen, D., Fischer, H., et al. (2012). Direct linking of Greenland and Antarctic ice cores at the Toba eruption (74 kyr BP). *Climate of the Past Discussions*, *8*, 5389–5427.